FULL PAPER

Benzodioxane-benzamides as antibacterial agents: Computational and SAR studies to evaluate the influence of the 7-substitution in FtsZ interaction

Valentina Straniero [a],*, Victor Sebastián Pérez[b], Martina Hrast[c], Carlo Zanotto[d], Andrea Casiraghi[a], Lorenzo Suigo[a], Irena Zdovc[e], Antonia Radaelli[d], Carlo De Giuli Morghen[f] and Ermanno Valoti[a]

[a] Dr. V. Straniero, orcid.org/0000-0002-5089-0879; Mr. A. Casiraghi, orcid.org/0000-0002-6256-5694, Mr. L. Suigo, orcid.org/0000-0002-8958-1547, Prof. E. Valoti, orcid.org/0000-0002-5608-3875
Department of Pharmaceutical Sciences
Università degli Studi di Milano
Via Luigi Mangiagalli 25, 20133 Milano, Italy
valentina.straniero@unimi.it

[b] Dr. V. Sebastián Pérez, orcid.org/0000-0002-8248-4496
Centro de Investigaciones Biológicas (CSIC)
Ramiro de Maeztu 9, 28040 Madrid, Spain

[c] Dr. M. Hrast, orcid.org/0000-0003-0488-2445
Faculty of Pharmacy
University of Ljubljana
Aškerčeva cesta 7, SI-1000 Ljubljana, Slovenia

[d] Dr. C. Zanotto, orcid.org/0000-0003-0222-6102, Prof. A. Radaelli, orcid.org/0000-0002-5683-6216;
Department of Medical Biotechnologies and Translational Medicine
Università degli Studi di Milano;
via Vanvitelli 32, 20129 Milano, Italy;

[e] Prof. I. Zdovc, orcid.org/0000-0002-5419-2779;
Faculty of Veterinary Medicine
University of Ljubljana
Gerbičeva 60, SI-1000 Ljubljana, Slovenia

[f] Prof. C. De Giuli Morghen, orcid.org/0000-0002-4127-3596;
Catholic University "Our Lady of Good Counsel",
Rr. Dritan Hoxha, Tirana, Albania.

Supporting information for this article is given via a link at the end of the document.

Abstract: FtsZ is a crucial prokaryotic protein involved in bacterial cell replication. It recently arose as a promising target in the search for antimicrobial agents able to fight antimicrobial resistance. In this work, going on with our SAR study, we develop differently 7-substituted 1,4-benzodioxane compounds, linked to the 2,6-difluoro-benzamide by a methylenoxy bridge. Compounds exhibit promising antibacterial activities not only vs multi drug resistant *Staphylococcus aureus*, but also on mutated *Escherichia coli* strains, thus enlarging their spectrum of action also towards Gram-negative bacteria. Computational studies elucidate, through a validated FtsZ binding protocol, the structural features of new promising derivatives as FtsZ inhibitors.

Introduction

Antimicrobial resistance is in continuous growing, reaching extreme levels. The World Health Organization (WHO) estimates by 2050 10 million deaths each year caused by this problem. This number definitely surpasses people died by cancer. [1]
This alarming progression renders commonly used antibiotics less or none effective. Novel molecules for the treatment of many bacterial infections are thus required.

Among the most common multi-drug resistant bacteria emerged *Staphylococcus aureus* (*Sa*). Indeed, *Sa* isolated from clinics revealed now not only to be resistant to methicillin, ampicillin, oxacillin and other β-lactam antibiotics, [2, 3] but also to a wider number of antibiotics, independently of their targets. Glycopeptides as vancomycin, [4] tetracyclines, aminoglycosides as gentamicin, lincosamides as clindamycin, macrolides as erythromycin, fluoroquinolones as ciprofloxacin and several other drugs showed their inefficacy towards *Sa*. [5]
Moreover, a large number of both Gram-positive, as *Enterococcus faecalis* [6] and *Streptococcus pneumonia* [7], and Gram-negative strains, as *Escherichia coli* (*E. coli*), [8] became resistant to the originally potent antimicrobials. This general inefficacy stressed the urgent need for the development of new antibacterial agents with an innovative and effective mechanism of action.

Among the possible targets, one critical process is the bacterial cell division and its crucial proteins, considering the essentiality of the division process in the growth and in the replication of bacterial cells. Filamentous temperature-sensitive protein Z (FtsZ) is one of the most promising, well-defined and druggable targets. It has a mandatory role in cell division, [9] is highly conserved in bacteria [10] and has less than 20% structural homology with human β-tubulin, even if they are functionally similar. Any perturbation on the protein proved deleterious on cytokinetic assembling and bacterial cell survival.

Starting from these considerations, in the last decade, a wide number of researchers focused their worked in the development of FtsZ inhibitors. The firstly discovered FtsZ compounds derived from natural molecules and from their structural modifications. Then, synthetic molecules gave better results; the most interesting antimicrobial classes were 3-alkoxylbenzamides

(**PC190723**, its derivative **TXY707** and the derived prodrugs **TXY541**, **TXY436** and **TXY709** in Figure 1), benzopyridines, pyrido- and pyrimido- pyrazines, benzimidazoles, naphtalenes and sulfonamides. [11-18] All these compounds proved their inhibition towards the prokaryotic protein, resulting in a bactericidal effect on a wide number of bacterial strains, especially Gram-positive ones.

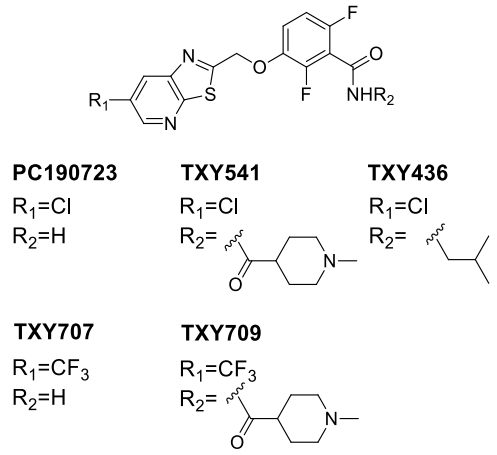

Figure 1 – Literature FtsZ inhibitors

Moreover, FtsZ crystal structures of different strains was intensively studied, alone or in association with known inhibitors, [19-22] and they were used as important starting points for designing novel inhibitors. In the latest years, our research group profusely investigate the SARs of different molecules, acting on peculiar biological targets. [23-26] In this context, we recently identified a copious class of FtsZ inhibitors. They potently inhibited both methicillin-sensitive and methicillin-resistant *S. aureus* and *M. tuberculosis*. [27-29]

Among them, the most interesting derivatives, here called **I**, **II** and **III**, [27,28] showed MIC vs MRSA between 0.5 and 0.6 µg/mL (see Figure 2). Morphometric analysis performed on *Sa* cells incubated with our derivatives showed the typical alterations of cell division inhibition.

Besides, we confirmed FtsZ as the target of this class of derivatives [29] using a GTPase activity assay and a polymerization activity assay. The two *in vitro* assays are the ones widely used to investigate changes in FtsZ enzymatic function, as suggested by Kusuma and Tripathy in recent reviews on this topic. [30, 31] FtsZ inhibition of PC190723 and of other FtsZ inhibitors was confirmed in this way.

Specifically, using the GTPase assay, we determined the effect of our derivatives on *Sa* FtsZ GTPase activity by incubating each compound with *Sa* FtsZ and by kinetically measuring inorganic phosphate release, as already seen for PC190723.
Conversely, we evaluated by SDS-page the increase in polymerization after the progressive addition of our derivatives (5, 10, and 20 µg/mL) and we quantified the percentage FtsZ in the pellets by densitometric analysis.

We assessed our class of compounds is able to modify the GTPase activity of *Sa* FtsZ and to stabilize FtsZ polymers, suppressing polymer dynamics and thus blocking bacterial cell division.

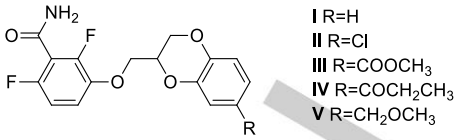

Figure 2 – Reference in-house FtsZ inhibitors

We profusely demonstrated the importance of the substituent in 7- position of the 1,4-benzodioxane ring, and we evaluated how the simplification of the estereal function (eluding one or the other Oxygen atoms as for **IV** and **V**) results in the maintenance of the antibacterial activity.

In this work, as a continuation of our SAR study and starting from reference compounds **III**, **IV** and **V**, we developed novel derivatives, modifying the substituent in position 7 of the 1,4-benzodioxane moiety and achieving compounds **1-11**.

Specifically, the carboxymethyl group was hydrolyzed obtaining the corresponding carboxylic acid (**1**). **1** was a versatile tool, used for its conversion into the morpholinamide (**2**) and for the bioisosteric replacement. Both the carboxymethyl and the carboxylic acid were substituted by introducing a tetrazole (**3**-**5**) or variously 5-substituted 1,2,4-oxadiazoles (**6**-**11**).

In addition to the synthesis and SAR study, we report a broader antibacterial activity. In detail, we tested the compounds against several Gram-positive *Sa* strains: methicillin sensitive, methicillin resistant and multi-drug resistant. Furthermore, we evaluate their activity not only vs Extended-spectrum beta-lactamase-positive *E. coli*, but also on mutated *E. coli* strains, as done for **PC190723** and its prodrug **TXY436**. [15] The best derivatives were also proved for their cytotoxicity towards human MRC-5 cells.

Moreover, we performed in silico studies, aimed at defining a docking protocol for this protein; we validated the model using the literature crystal structures of **PC190723** and **TXY707** and we then applied the protocol on our compounds. Hotspots analysis were accomplished to identify the main binding pockets in the protein and the main key interactions for each binding cavity. Docking studies allow us to decipher the binding mode of our family of derivatives and to define the chemical and structural properties of the binding cavity.

Besides, calculations of a huge number of physicochemical properties revealed the general good profile in terms of drug-like properties for the vast majority of the compounds.

Chemistry

Compounds **1-11** (Figure 3) were designed starting from the chemical structures of **III**, **IV** and **V**.
The general synthetic pathway for their synthesis is shown in the Scheme 1 and it started from the commercially available 3,4-dihydrobenzoic acid for all the derivatives. The synthesis for each compound follows a particular branch that is better explained and reported in Scheme 2, Scheme 3 and Scheme 4.
The first common step for whole series of compounds (see Scheme 2) is the esterification of the starting carboxylic acid (**12**) and the consecutive reaction with epibromohydrin, yielding the 7-substituted intermediate (**13**). The 6- substituted isomer was

obtained only in traces, which were successfully removed via purification by flash chromatography. In order to achieve 1, compound 13 was firstly mesylated (**14**) and sequentially reacted with 2,6-difluoro-3-hydroxybenzamide, accomplishing the intermediate **15**, which was then hydrolyzed under basic and warm conditions, achieving **1** as a white solid.

The simple condensation of **1** with morpholine, in the presence of HOBt and EDC hydrochloride as coupling agents, produce the compound **2** in quantitative yields. The synthesis of the bioisosters **3-11** differ from one product to the other, but required the accomplishment of a common intermediate, **18** (see Scheme 3). For its obtainment, the 7-substituted intermediate **13** underwent the simultaneous protection of the hydroxyl function with benzyl bromide and the hydrolysis of the ester, yielding **16**. Its carboxylic function was converted into the primary amide **17**, via formation of the acyl chloride. The sequential treatment with TFAA allow the dehydration and the consecutive formation of the nitrile group, obtaining **18**.

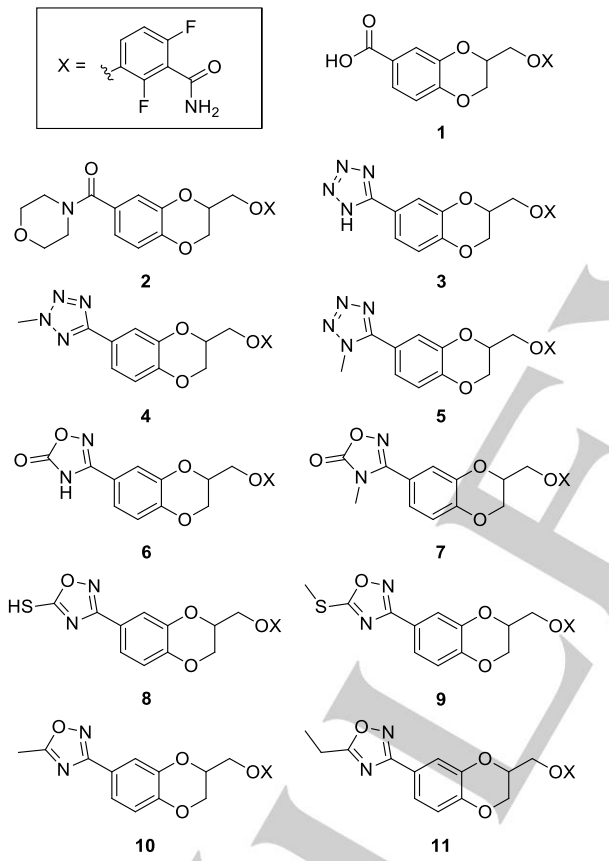

Figure 3 – Compounds object of the present work

The three tetrazoles **3-5** were prepared from **18**, following two different pathways, as reported in Scheme 1. In case of **3** (better explained in Scheme 4), the intermediate **18** was firstly debenzylated (**19**) and mesylated (**20**), then reacted with 2,6-difluoro-3-hydroxybenzamide (**21**) and finally treated with sodium azide. This last step let the conversion of the nitrile function into the tetrazole ring and thus the accomplishing of **3.**

On the other hand (see Scheme 4), in case of **4** and **5**, the tetrazole **22** was formed from the nitrile function, treating **18** with sodium azide as previously done. This was further methylated, obtaining both the 1- and 2- substituted tetrazoles **23** and **24**. The two intermediates were isolated by flash chromatography and characterized by NMR, their ^{1}H-NMR were significantly diverse and such a difference let to define the right methylation position on the tetrazole ring. Specifically, the chemical shift of the methyl group was of 4.15 ppm for derivative **23** and of 4.37 ppm for **24**. Literature data [32,33] helped us in the identification of the two compounds. In particular, the ratio between the 1- and the 2-methyl tetrazole derivatives resulted to be of 25/75, respectively. **23** and **24** followed the same synthetic pathway, consisting in the debenzylation of the ether (**25** and **26**) and the consequent mesylation of the hydroxyl function, affording **27** and **28**, and the final reaction with 2,6-difluoro-3-hydroxybenzamide, obtaining 4 and **5**.

Scheme 1 – General synthetic pathway for the synthesis of **1-11**

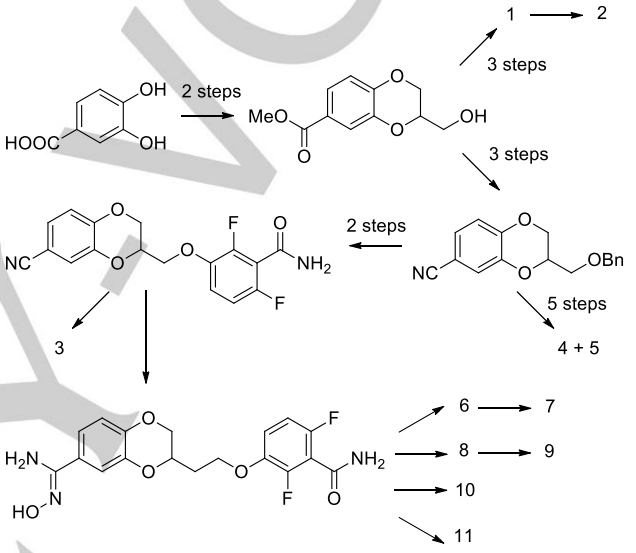

Scheme 2 – Synthesis of **1** and **2**

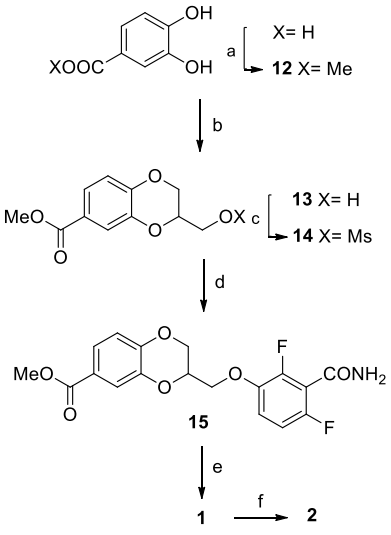

Reactives and solvents: (a) $SOCl_2$, trimethyl ortoformate, MeOH, reflux; (b) epibromohydrin, TEA, DCM, RT; (c) Mesyl chloride, TEA, DCM, RT (d) 2,6-Difluoro-3-hydroxybenzamide, K_2CO_3, DMF, 80°C; (e) NaOH, MeOH, 50°C; (f) morpholine, HOBt hydrate, EDC*HCl, DIPEA, DCM, RT.

Scheme 3 – Synthesis of **18**

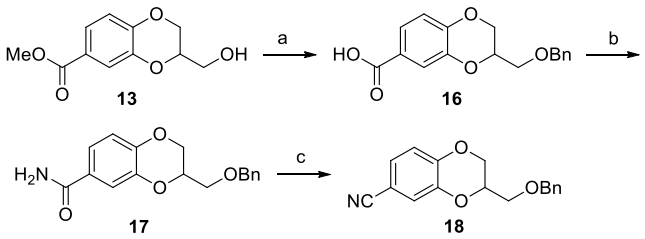

Reactives and solvents: (a) I. Benzyl bromide, NaH, THF, reflux; II. NaOH, MeOH, 50°C; (b) I. $SOCl_2$, 50°C; II. NH_3 30%, DCM, RT; (c) TFAA, dioxane, pyridine, RT.

The synthesis of **6**-**11** required an additional common intermediate, called **29** (see Scheme 5), which was easily obtained from **21**, through treatment with hydroxylamine hydrochloride in basic conditions. Starting from **29**, **6** and **8** were quickly obtained through treatment with CDI and TCDI, respectively, in the presence of DBU as a base. The methylated derivatives **7** and **9** were obtained from treatment of **6** and **8** with methyl iodide.

Even **10** and **11** were easily accomplished from **29**, treating it firstly with acetic or propionic anhydride, in a suitable solvent, and then with NaOH, in order to let the cyclization into the required ring.

Scheme 4 – Synthesis of **4** and **5**

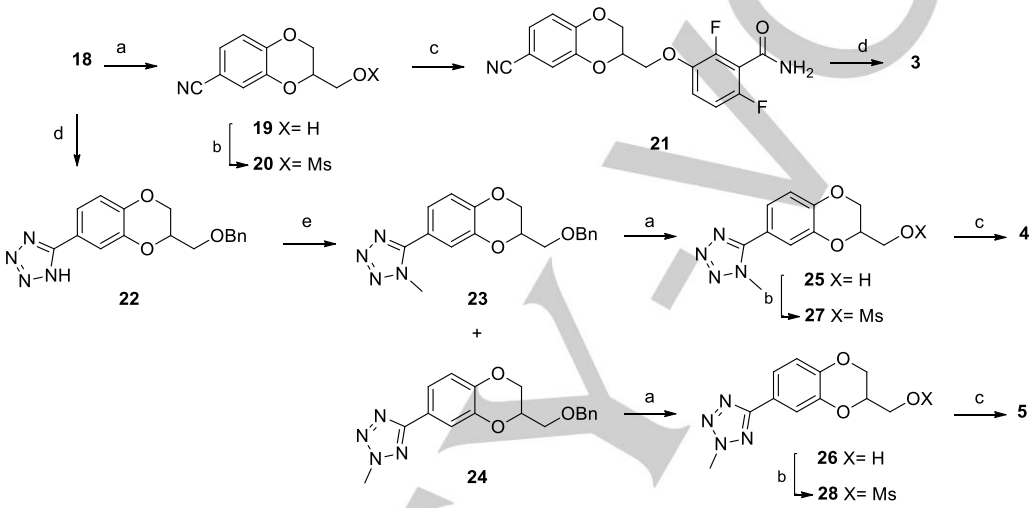

Reactives and solvents: (a) BBr_3, DCM, 0°C; (b) Mesyl chloride, TEA, DCM, RT; (c) 2,6-Difluoro-3-hydroxybenzamide, K_2CO_3, DMF, 80°C; (d) NaN_3, $ZnCl_2$, H_2O/DMF, reflux; (e) MeI, K_2CO_3, DMF, 50°C.

Scheme 5 – Synthesis of **6-11**

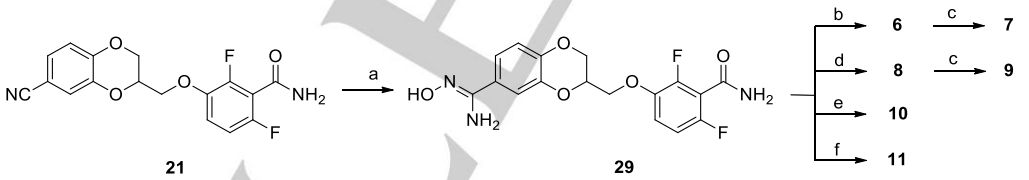

Reactives and solvents: (a) NH_2OH*HCl, K_2CO_3, EtOH/H_2O, reflux; (b) CDI, DBU, ACN, reflux; (c) MeI, K_2CO_3, ACN/DMF, 45°C; (d); TCDI, DBU, ACN, reflux; (e) I. acetic anhydride, DCM, RT; II. NaOH, DMF, RT; (f) I. propionic anhydride, ethyl acetate, RT; II. NaOH, DMF, RT.

Results and Discussion

We initially tested compounds **1**-**11** as done for the reference compounds **III**, **IV** and **V**, as a continuation of our previous studies. Specifically, we chose a methicillin-sensitive *S. aureus* (MSSA, ATCC 29213) and a methicillin-resistant *S. aureus* (MRSA, ATCC 43300) as Gram-positive bacteria and an extended-spectrum of beta-lactamase-positive (ESBL) *E. coli* as Gram-negative one (Table 1). Their inhibitory ability was evaluated determining the MIC, i.e. the lowest compound dose (μg/mL) at which growth is inhibited, as well as the Minimal Bactericidal Concentration (MBC), i.e. the minimal dose (μg/mL) at which cell growth is irreversibly blocked after compound removal. The compounds showing the most promising activities vs MRSA were also assessed for their cytotoxicity on human MRC-5 cells. We determined TD90 as the concentration (μg/mL) able to reduce by 90% the viability of these cells; furthermore, we calculated the therapeutic index (TI), expressed as the ratio between TD90 and MBC values.

When tested on ESBL *E. coli*, none of the compounds resulted in inhibiting cell growth at 100 μg/mL, which was the highest dose proven. These data were in line with previously obtained results for the reference compounds **III**-**V**, suggesting a complete inactivity on this strain, even modifying the substituent in 7-position on the 1,4-benzodioxane ring (Table 1).

Differently, the MSSA and MRSA inhibition values were promising and interesting, considering the distinctive behavior of structurally similar compounds.

Derivative **9** resulted to have the most promising antibacterial activities (see Table 1). We conducted morphometric analyses

(Figure 4) to assess its effect on bacterial cell division process, showing significant alterations in cellular dimension. Bacterial swelling and cell desegregation commonly resulted in cytocidal activity.

Specifically, by light microscopy (upper images in Figure 4), we observed an increase in cell volume of *S. aureus*, when cultured in the presence of **9** and difluorononyloxy benzamide (DFNB) [34] as reference FtsZ inhibitor (positive control). No morphological changes were noticed in untreated *S. aureus*.

The same morphometric changes were confirmed by transmission electron microscopy (lower images in Figure 4), which showed also alterations in the septum formation and bacterial desegregation, with consequent loss of the cytoplasmatic content.

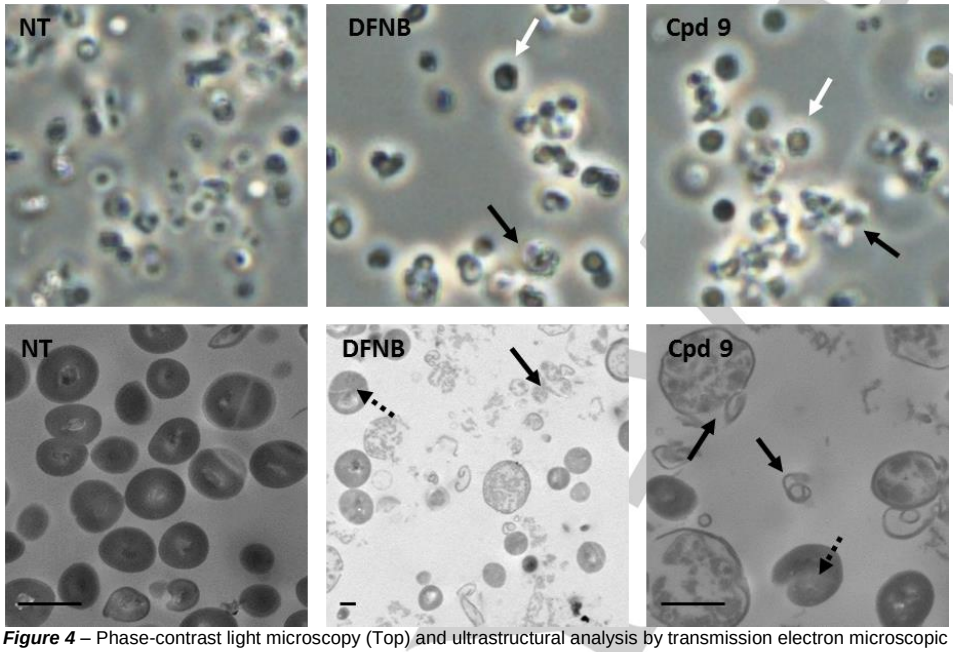

Figure 4 – Phase-contrast light microscopy (Top) and ultrastructural analysis by transmission electron microscopic (Bottom) of *S. aureus* after overnight incubation: Cells with no compound (NT as negative control); cells in the presence of compound **DFNB** (0.25 µg/mL) as positive control and of compound **9** (0.6 µg/mL). Scale bar: 1 micron. Desegregations and loss of cytoplasmatic content: black solid arrows; bacterial swelling: white arrows; alterations in septum formation: black dashed arrows.

MSSA and MRSA inhibition values of all the derivatives, reported in Table 1, give interesting insights in their SAR.

Indeed, the simple transformation of the methyl ester of **III** into the carboxylic acid **1** or into the morpholinamide **2** resulted in the complete loss of activity.

The detrimental result of the free carboxylic acid **1** underlined how the inhibitory potency of **III** was strictly related to the maintenance of the ester moiety, and not to the supposed metabolic hydrolytic product.

Furthermore, compound **2** was suitably designed from **III** as morpholine amide in order to include in its structure peculiar requirements. Firstly, the replacement of the Oxygen atom with the Nitrogen one as isoster. Secondly, the insertion of a disubstituted amide in order to avoid any competition with the active site of the 2,6-difluorobenzamide and, at the same time, to keep to ability of acting as HBA, as the reference ester **III**. Unfortunately, the loss of antibacterial activity of **2** confirmed the importance of hydrophobic substituents in 7- position of the benzodioxane moiety, similarly with what previously obtained for 7- butyl aminocarbonyl derivative. [24] Moreover, in order to better elucidate the importance of the methyl ester of **III**, we introduced different 5-membered rings, in their free or methylated species (see compound **3-11**, Figure 3), which are commonly used as bioisosters of the carboxylic and carboxymethyl function, respectively.

Considering tetrazoles **3** (bioisoster of the carboxylic acid **1**) and **4, 5** (both bioisosters of the methyl ester **III)**, the presence of the methyl group resulted in two opposite effects on antimicrobial activity. Specifically, compound **4**, having the methyl in position 2-, revealed to be a potent inhibitor, while **5**, with the methyl in position 1-, is even less active than the tetrazole **3**.

It is suggested that the difference in antimicrobial activity could be a consequence of the substitution position and thus of the steric hindrance of the methyl group, which affects FtsZ interaction.

In case of **3**, the maintenance of the weak inhibitory activity could be justified by the charge delocalization of the tetrazole ring that influences the tautomeric balance, thus affecting the whole lipophilicity of the molecule. The formation of both the two regioisomers (**4** and **5**), during alkylation reaction, corroborated our hypothesis.

A similar behavior was seen also for the bioisosteric 5-substituted oxadiazoles **6-11**. Particularly, non-methylated rings **6** and **8** showed a loss of the antimicrobial activity. Conversely, methylated oxadiazoles gave also in this case two different results: **7** was completely inactive, while **9-11** brought promising results.

The just mentioned differences in FtsZ interaction of the methylated oxadiazoles, and consequently the discrepancy in the inhibitory activities, confirmed the importance of the substitution position. Specifically, when the methyl is close to the 1,4-benzodioxane, as for **7**, the derivative is inactive. Otherwise, the presence of 2- methylated rings, as for **9**, **10** and **11**, results in potent antimicrobial agents.

Table 1. Inhibitory activity of compounds **III-V** and **1-11** against MSSA, MSSA and MRC-5

Cpd	*MSSA ATCC 29213*			*MRSA ATCC 43300*			*MRC-5*	*ESBL E. coli*
	MIC (µg/mL)	MBC (µg/mL)	TI	MIC (µg/mL)	MBC (µg/mL)	TI	TD90 (µg/mL)	MIC (µg/mL)
III	0.6	0.6	> 1280	N.D	N.D.	/	> 800	> 100
IV	2.5	5	> 160	2.5	5	> 160	> 800	> 100
V	5	10	40	5	10	40	400	> 100
1	> 100	> 100	/	> 100	> 100	/	/	> 100
2	> 100	> 100	/	> 100	> 100	/	/	> 100
3	80	100	/	80	100	/	/	> 100
4	2.5	2.5	36	2.5	2.5	36	90 ± 0.7	> 100
5	> 100	> 100	/	> 100	> 100	/	/	> 100
6	> 100	> 100	/	> 100	> 100	/	/	> 100
7	> 100	> 100	/	> 100	> 100	/	/	> 100
8	> 100	> 100	/	> 100	> 100	/	/	> 100
9	0.6	0.6	1184	0.6	0.6	1184	740 ± 0.17	> 100
10	2.5	2.5	> 320	2.5	2.5	> 320	> 800	> 100
11	2.5	2.5	> 320	2.5	2.5	> 320	> 800	> 100

In order to confirm the importance of the structural features in the interaction with FtsZ and consequently in the antibacterial potency, we followed a diverse approach.

Using computational studies, we aimed at deciphering the potential binding mode of this family of derivatives and at gaining more insights into the binding cavities of *Sa* FtsZ protein. At the same time, we performed an analysis considering the main pharmaceutical relevant properties of these derivatives, in order to study their drug-likeness. With the objective of obtaining more information related to the main catalytic pocket in the protein as well as identifying potential additional binding cavities, hotspot analysis was carried out. According to the results obtained using Fragment Hotspots maps application, [35] two druggable binding pockets were identified; these pockets are the GTP binding site and the ligand binding site. Both pockets showed a hydrophobic profile depicted with the yellow hotspot and several additional polar hotspots represented in blue and red (Figure 5).

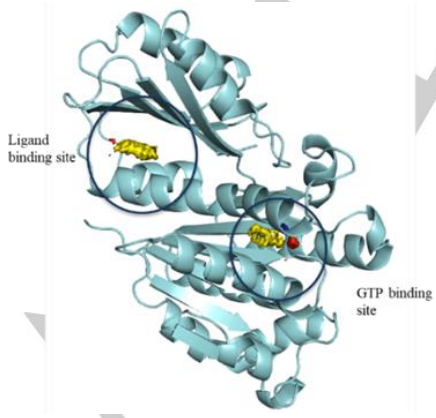

Figure 5 – Hotspots analysis of the FtsZ protein. 2 pockets were identified, the ligand and the GTP binding site (left and right side of the protein, respectively)

For this study, we are going to focus mainly on the ligand binding site since previous studies have identified this pocket as the cavity in which most of the ligands containing 2, 6-difluorobenzamide moiety bind. The hotspots results will allow us to assess the binding interactions of the docking studies. Considering the hotspots results, it will be possible to further identify and design novel derivatives that meet the interactions criteria.

Before carrying out the docking studies, our first aim was the definition and the consequent validation of the docking protocol for FtsZ, in order to decipher the binding mode of the class of compounds described in this work. For this purpose, two potent inhibitors, PC190723 and TXA707 that had been previously crystallized with the FtsZ protein of S. aureus (PDB code: 4DXD [14] and 5XDT [22]) were considered as reference compounds. Moreover, the two compounds crystallized (PC190723 and TXA707 respectively) contained a 2,6-difluorobenzamide moiety, also found in the chemical family described in this work. For this reason, both compounds were redocked into the binding site of the FtsZ crystal structure. As a result, the poses obtained from the docking studies were almost identical to the ones found in the crystal structures (Figure 6). Moreover, it is important to remark that the main interactions, three key hydrogens bonds with Val207, Leu209 and Gln263, are maintained in the docking results compared with the crystal structure. Additionally, the hydrophobic interaction profile is also very similar. These results validate the docking protocol, which will be further applied in the docking studies.

Once the protocol was validated, the binding mode of the compounds synthesized in this work was assessed. In order to optimize the active site of the protein considering this new chemical family of benzodioxane derivatives, an induced fit docking study was performed with the most potent compound of this series (compound **9**). This docking method allows conformational changes in the lateral chains of the residues that are part of the binding site induced by the bound ligand. According to the results, it is possible to confirm the three key hydrogen bonds between the 2, 6-difluorobenzamide moiety and the FtsZ protein. On the other hand, modeling data highlighted the specific FtsZ region involved in binding the benzodioxane scaffold. This

scaffold extends its conformation towards the inner part of the pocket and the benzodioxane substituent, the 5-membered ring moiety, is inserted into the deepest part of the cavity characterized by its narrowness and hydrophobicity. [22] These chemical features that characterized the binding mode of these derivatives can be observed in Figure 7. The docking results for the rest of the active derivatives such as compound **4**, **10** or **11** revealed, as expected, very similar binding poses compared to reference compound **9**. In this sense, the 5-membered ring substituent is accommodated in the inner hydrophobic subpocket surrounded by hydrophobic residues such as Met98, Phe100, Val129, Ile162, Gly193, Ile197, Val214, Met218, Met226, Leu261 and Ile311. The high hydrophobicity of this subpocket suggests that polar substituents in the benzodioxane moiety are not well tolerated. This finding might explain the absence of activity of molecules containing a hydrophilic substituent such as the ones that are present in compounds **1**, **2**, **3** and **6-8**.

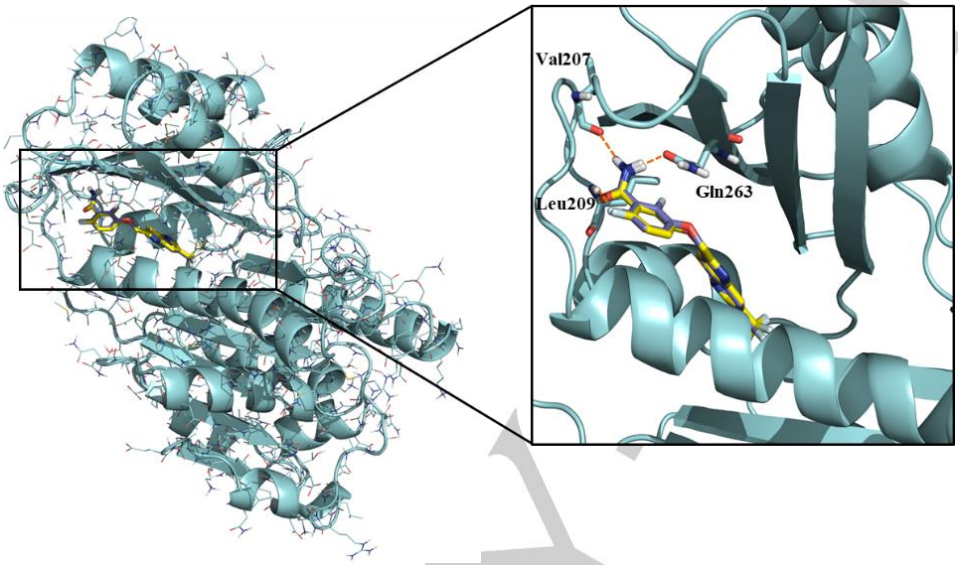

Figure 6 - TXA707 docking results in the crystal structure of FtsZ 5XDT. A superposition of the ligand in the crystal structure (purple) and the results of the docking studies (yellow) are depicted

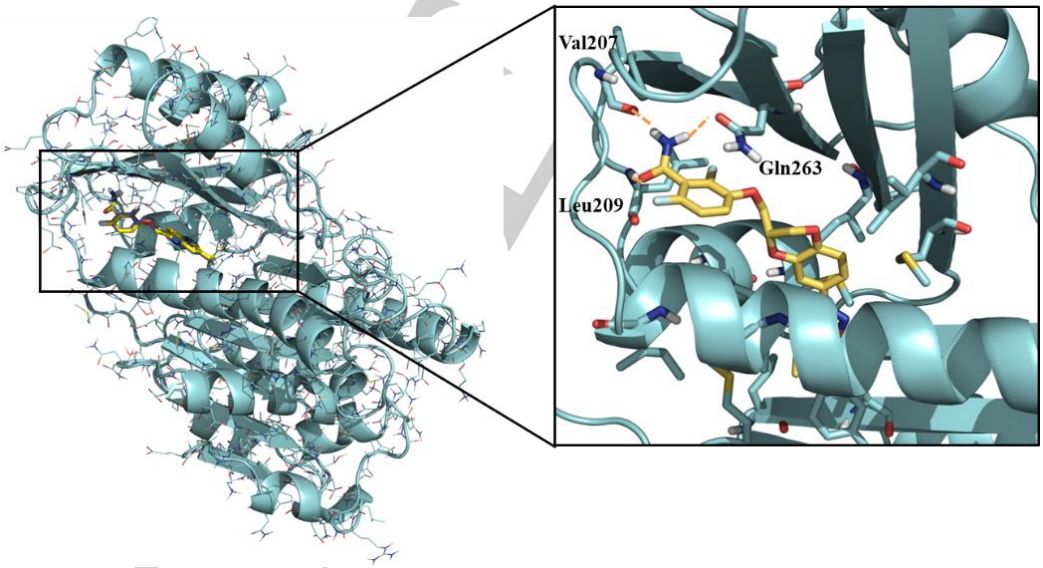

Figure 7 - Binding mode of the most active compound, **9**, of this family of derivatives

Also, the narrowness of the pocket and its steric restrictions might explain that substitutions in position 1 of the 5-membered ring are not preferred such as in compound **5** compared to 2 substituents (compound **4**). The former is indeed more linear and less steric hindered than the latter, which therefore seems to be not tolerated by the task. The general steric requirements of the cavity can also validate the promising activities of compounds **9-11**, differently from the null inhibition of **7**.

Additionally, we calculated *in silico* the most significant physical-chemical and drug-like properties of this class of compounds, in order to achieve further information and to understand any influence on cellular activity and FtsZ inhibition. Table 2 reports the calculations of the following predicted parameters: dipole moment of the molecule (Dipole), octanol/water partition coefficient (QPlogPo/w), apparent Caco-2 cell permeability in nm/sec (QPPCaco) and apparent MDCK cell permeability in nm/sec (QPPMDCK).

Table 2. Key drug-like and permeability properties calculated for this family of compounds.

Cpd	Dipole	QPlogPo/w	QPPCaco	QPPMDCK
III	9.399	2.663	295.021	321.39
IV	10.188	2.809	384.081	427.37
V	5.871	3.073	1.036.487	1249.93
1	9.115	2.223	26.502	30.202
2	10.805	2.490	460.630	520.197
3	13.998	1.543	61.419	58.907
4	6.783	2.279	201.657	213.008
5	13.311	2.23	118.901	120.357
6	15.685	1.250	38.547	35.623
7	11.064	1.831	75.493	73.685
8	8.206	2.701	233.639	745.038
9	8.596	3.173	305.372	628.525
10	6.78	2.55	249.607	268.238
11	6.657	2.96	290.952	316.567

Considering these results, the general in silico permeability profiles confirmed that the higher the permeability values are, the more potent are the derivatives. Regarding dipole values, it is important to remark the relationship between high dipole values and low antibacterial activity, such as in the case of compounds **3**, **5**, **6** and **7**. According to the recommended values by the Qikprop software, [36] the higher the computed dipole moment is (mainly above 12), the lower the ability to show properties in the range of drug-like compounds. Moreover, the high dipole value of **5**, confirms the initial suggestion about its inactivity, which was previously explained in terms of steric hindrance in the target-approach. Despite the high similarity between **4** and **5**, there is a great difference in terms of dipole values, suggesting that 4 displays better drug-like properties with a better permeability profile. Similarly, the inactivity of derivative **6** and **7** is demonstrated not only by the inadequate presence of a hydrophilic 5-membered ring substitution for the interaction profile in the enzyme, but also by the low permeability profile combined with the high dipole values.

The promising drug-like properties of this class of derivatives, together with the interesting data on MRSA and MSSA, prompted us in enlarging the Gram-positive strains to be tested. We firstly evaluated the derivatives on two clinical isolates of *S. aureus*, called MRSA 12.1 and MRSA 11.7, which show resistance towards antibiotics belonging to different classes and thus directed to disparate targets. MRSA 12.1 is resistant to gentamicin, kanamycin, rifampicin, streptomycin, sulfamethoxazole and tetracycline, while MRSA 11.7 proved its resistance vs ciprofloxacin, clindamycin, erythromycin, quinupristin and dalfopristin in association, tetracycline, tiamulin and trimethoprim.

Table 3 reports the obtained antimicrobial activities, expressed as MICs. Data show how **4**, **9**, **10** and **11** confirmed their promising activity, and thus their potentiality towards these multi-drug resistant strains.

Table 3. Inhibitory activity of compounds **III-V** and **1,3-5**, **9-11** against MRSA 12.1 and MRSA 11.7

Cpd	MRSA 12.1	MRSA 11.7
	MIC (µg/mL)	MIC (µg/mL)
III	≤ 1	≤ 1
IV	4	8
V	4	4
1	> 128	> 128
3	> 128	> 128
4	4	4
5	> 128	> 128
9	≤ 1	≤ 1
10	2	4
11	2	4

Moreover, the good permeability profiles of most of our novel derivatives encourage us to explore more in depth also Gram-negative strains.

Indeed, the promising permeability values (in particular the ones of **V**, **2**, **4**, **8-11**) seem to be in conflict with their intrinsically inactivity on ESBL *E. coli*, prompting us in evaluating suitably mutated strains. Indeed the two strains, *E. coli* D22 and *E. coli* N43, are characterized by differences in permeability and in bacterial cell drug-retention, respectively.

Specifically the former bears a mutation in the LpxC gene that increases membrane permeability, while the latter is knockout of AcrAB cell membrane pump.

Since the poor activity on *E. coli* ESBL may reflect an inability of our compounds to target *E. coli* FtsZ effectively, we aimed in understanding if the reason could be due to an impossibility to penetrate Gram-negative membrane or, as for PC190723 and its prodrug TXY436 [15], to being a substrate of the resistance-nodulation-cell division (RND)-type efflux pump AcrAB.

Table 4. Inhibitory activity of compounds **III-V** and **1,3-5, 9-11** against mutated *E. coli*

Cpd	*E. coli* D22	*E. coli* N43
	MIC (µg/mL)	MIC (µg/mL)
III	> 128	16
IV	> 128	32
V	> 128	64
1	> 128	> 128
3	> 128	> 128
4	> 128	32
5	> 128	> 128
9	> 128	16
10	> 128	16
11	> 128	32

The resulting MICs, summarized in Table 4, revealed how only **1**, **3** and **5** confirm their complete inactivity towards these mutated

Gram-negative bacteria, as previously seen for Gram-positive *Sa* strains, due to their structural features.

On the contrary, the other derivatives, together with the reference compounds **III**, **IV** and **V**, resulted active, with antimicrobial potency almost comparable to the one shown by TXY436. It suggests that **III**, **IV**, **V**, **4**, **9**, **10** and **11**, as well as TXY436, are substrates of the AcrAB efflux pump and that they are thus able to target FtsZ function and disrupt cell division also in this bacterium.

Conclusions

The aims of the present work could be summarized as follows: 1) deepening the SAR analysis of this chemical class, starting from reference compound **III**; 2) enlarging the variety of bacterial strains; 3) performing a computation study in order to better elucidate the FtsZ binding site features; 4) understanding the reasons of inactivity towards Gram-negative E. coli.

Among all the synthetized derivatives, we obtained a series of potent bioisosters of **III**. The correlation of the chemical structures with the antimicrobial activities, the predicted physical chemical properties and docking analysis let us observing that both the molecular dipole value and the molecular shape are directly related to the bactericidal properties.

Indeed, also the molecular geometry, and specifically the presence of regioisomers, revealed to be determinant in FtsZ interaction. The strong differences in antimicrobial activity between **4** and **5**, **7** and **9-11** highlighted both the permeability issue and that some substituents are not well tolerated by the FtsZ binding cavity. This consideration will be useful for further structural modifications, because it help us in defining the chemical requirements of a potent FtsZ inhibitor with antimicrobial cellular activity.

Finally, the whole results coming from the Gram-negative strains highlights the capability of these compounds to penetrate *E. coli* membrane and to have an antibacterial activity on this bacteria. The genetic inactivation of RND-type efflux pump AcrAB renders these derivatives as potent as PC190723 on this pathogen, confirming that they are substrates of the efflux pump.

Experimental Section

Chemical synthesis

All starting materials were obtained from commercial suppliers and used without further purification. ^{1}H and ^{13}C NMR spectra were taken on Varian 300 Mercury NMR spectrometer operating at 300 MHz for ^{1}H NMR, and 75 MHz for ^{13}C NMR. Chemical shifts (δ) are reported in ppm relative to residual solvent ($CDCl_3$ or DMSO-d_6) as internal standard. Signal multiplicity is used according to the following abbreviations: s= singlet, d= doublet, dd= doublet of doublets, t= triplet, td= triplet of doublets, q= quadruplet, m= multiplet, sept= septuplet and bs= broad singlet.. Silica gel F254 was used in analytical thin-layer chromatography (TLC), and silica gel (particle size 40-63 µm, Merck) was used in flash chromatography; visualizations were accomplished with UV light (λ 254 nm). Melting point were determined by DSC (Q20 TA INSTRUMENTS) or Büchi Melting Point (B-540). Elemental analyses of the new substances are within 0.40% of theoretical values, therefore the purity of all the final products proved to be ≥95%.

ABBREVIATIONS

CDI= 1,1'-Carbonyldidimidazole, DBU= 1,8-Diazabicyclo[5.4.0]undec-7-ene, DCM= Dichloromethane, DIPEA= N,N-Diisopropylethylamine, DMF= N,N-Dimethylformamide, DMSO= Dimethyl sulphoxide, EDC*HCl= N-(3-Dimethylaminopropyl)-N′-ethyl carbodiimide hydrochloride, HOBt= 1-Hydroxybenzotriazole hydrate, TCDI= 1,1′-Thiocarbonyldiimidazole, TEA= Triethylamine, TFAA= Trifluoroacetic anhydride, THF= Tetrahydrofuran.

General Procedure for Mesylation (Method A). Mesyl chloride (1.30 equiv) was added dropwise to a solution of the alcohol (1.00 equiv) and TEA (1.30 equiv) in DCM (15 mL) at 0 °C. The mixture was stirred at that temperature for 1 to 3 hours, diluted with DCM (20 mL), washed firstly with 10% aqueous $NaHCO_3$ (10 mL), secondly with 10% aqueous HCl (10 mL) and finally with 10% aqueous NaCl (10 mL), dried over Na_2SO_4, filtered and concentrated under vacuum to give a residue, which was used as crude or purified by flash chromatography on silica gel.

General Procedure for the Final Condensation (Method B). Potassium carbonate (1.10 equiv) was added to a solution of 2,6-difluoro-3-hydroxybenzamide (1.05 equiv) in dry DMF (5 mL). After stirring at room temperature for 30 min, a solution of the mesyl derivative (1.00 equiv) in DMF (5 mL) was added. The reaction mixture was stirred at 80 °C for 16h, concentrated under vacuum, diluted with Ethyl Acetate (15 mL), washed with brine (3x10 mL), dried over Na_2SO_4, filtered and concentrated, to give a residue, which was purified by flash chromatography on silica gel and/or by crystallization.

General Procedure for the Debenzylation (Method C). BBr_3 1.0 M in DCM (1.00 equiv) was added dropwise to a solution of the benzyl ether (1.00 equiv) in DCM (5/10 mL) at -5 °C. The mixture was stirred at -5 °C for 2 hours, then it was diluted with DCM (10 mL) and quenched with 10% aqueous $NaHCO_3$ (10 mL), stirring at 0 °C for 20 minutes. The organic layer was then dried over Na_2SO_4, filtered and concentrated under vacuum.

General Procedure for the Methylation (Method D). Potassium carbonate (1.20 equiv) was added to a solution of the tetrazole in DMF or ACN (10 mL). After stirring for 30 minutes at room temperature, methyl iodide (1.20 equiv) was added dropwise. The reaction mixture was stirred at 50 °C for 3 to 18 hours, concentrated under vacuum, diluted with Ethyl Acetate (10 mL), washed firstly with 10% aqueous $NaHCO_3$ (1x10 mL), secondly with 10% aqueous NaCl (1x10mL), dried over Na_2SO_4, filtered and concentrated to give a residue, which was purified by flash chromatography on silica gel.

Methyl 3,4-dihydroxybenzoate (12): Trimethyl orthoformate (3.9 mL, 35.68 mmol) and thionyl chloride (4.73 mL, 64.88 mmol) was added to a solution of 3,4-dihydroxybenzoic acid (5 g, 32.44 mmol) in methanol (50 mL) at 0 °C. The reaction mixture was heated at reflux and stirred for 16 hours, concentrated under vacuum, diluted with Ethyl Acetate (50 mL), washed firstly with 10% aqueous $NaHCO_3$ (2x15 mL), secondly with 10% aqueous NaCl (2x15 mL), dried over Na_2SO_4, filtered and concentrated, to give 4.36 g of 12 (80%) as a white solid. mp: 130 °C. ^{1}H NMR (300 MHz, $CDCl_3$): δ 7.64 (d, J = 2.0 Hz, 1H), 7.57 (dd, J = 8.3, 2.0 Hz, 1H), 6.91 (d, J = 8.3 Hz, 1H), 3.89 (s, 3H) ppm.

Methyl 3-(hydroxymethyl)-1,4-benzodioxan-6-carboxylate (13): Potassium Carbonate (4.30 g, 31.11 mmol) was added to a solution of **12** (4.36 g, 25.93 mmol) in DMF. After stirring at room temperature for 1 hour, epibromohydrin (2.66 mL, 31.11 mmol) was added. The reaction mixture was stirred at 40 °C for 18 hours, concentrated under vacuum, diluted with Ethyl Acetate (50 mL), washed firstly with 10% aqueous NaCl (1x30 mL), secondly with 10% aqueous NaOH (1x30 mL) and finally with 10% aqueous NaCl (1x30 mL), dried over Na_2SO_4, filtered and concentrated, to give 4.6 g of 13 (79%) as a yellow oil. ^{1}H NMR (300 MHz, $CDCl_3$): δ 7.58 (m, 2H), 6.91 (dd, J = 8.7, 4.2 Hz, 1H), 4.36 (dd, J = 11.1, 2.1 Hz, 1H), 4.26 (m, 1H), 4.16 (dd, J = 11.1, 7.8 Hz, 1H), 3.93 (dd, J = 12.1, 4.1 Hz, 1H), 3.87 (s, 3H), 3.85 (dd, J = 12.1, 1.5 Hz, 1H) ppm.

Methyl 3-(methylsulfonyloxymethyl)-1,4-benzodioxan-6-carboxylate (14): Method A from **13** (4.6 g, 20.52 mmol), purifying the crude by flash chromatography on silica gel and eluting with 7/3 Cyclohexane/Ethyl

Acetate, giving 5.65 g (91%) of 14 as a yellow oil. ^{1}H NMR (300 MHz, $CDCl_3$): δ 7.59 (m, 2H), 6.93 (dd, J = 8.9, 2.0 Hz, 1H), 4.52 (m, 3H), 4.36 (m, 1H), 4.15 (m, 1H), 3.88 (s, 3H), 3.10 (s, 3H) ppm.

2,6-Difluoro-3-(7-methoxycarbonyl-1,4-benzodioxan-2-yl)methoxybenzamide (15): Method B from **14** (1.25 g, 4.15 mmol), purifying the crude by crystallization from methanol and yielding 0.45 g (29%) of **15** as a white solid. mp= 154.7 °C. ^{1}H NMR (300 MHz, $CDCl_3$): δ 7.59 (m, 2H), 7.08 (td, J = 9.1, 5.2 Hz, 1H), 6.90 (m, 2H), 5.99 (bs, 2H), 4.58 (m, 1H), 4.46 (dd, J = 11.5, 2.4 Hz, 1H), 4.36–4.18 (m, 3H), 3.88 (s, 3H) ppm.

2,6-Difluoro-3-(7-carboxy-1,4-benzodioxan-2-yl)methoxybenzamide (1): 10% aqueous Sodium hydroxide (0.8 mL, 2 mmol) was added to a solution of **15** (0.3 g, 0.79 mmol) in methanol (8 mL). The reaction mixture was stirred at 50 °C for 4 hours, concentrated under vacuum and diluted with DCM and H_2O. The further treatment of the aqueous phase with concentrated HCl let the precipitation of 0.27 g of 1 (92%) as a white solid. mp: 219°C with partial decomposition. ^{1}H NMR (300 MHz, d_6-DMSO): δ 12.74 (bs, 1H), 8.13 (bs, 1H), 7.86 (bs, 1H), 7.43 (m, 2H), 7.30 (td, J = 9.4, 5.3 Hz, 1H), 7.06 (m, 2H), 4.63 (m, 1H), 4.51 (dd, J = 11.6, 2.2 Hz, 1H), 4.34 (m, 2H), 4.19 ppm (m, 1H). ^{13}C -NMR (75 MHz, d_6-DMSO): δ 167.1, 161.7, 152.6 (dd, J = 240.2, 6.7 Hz), 148.4 (dd, J = 247.2, 8.3 Hz), 147.3, 143.1 (dd, J = 10.8, 2.9 Hz), 142.6, 124.6, 123.6, 118.7, 117.5, 117.1 (dd, J = 24.9, 20.2 Hz), 116.3 (d, J = 9.1 Hz), 111.5 (dd, J = 22.7, 3.6 Hz), 71.7, 68.6, 65.2 ppm. Elemental analysis calculated (%) for $C_{17}H_{13}F_2NO_6$: C 48.41; H 6.38; N 4.03. Found: C 48.35; H 6.50; N 3.97.

2,6-Difluoro-3-(7-(N-morpholylcarbonyl)-1,4-benzodioxan-2-yl)methoxybenzamide (2): DIPEA (0.15 mL, 0.86 mmol) was added dropwise to a solution of 1 (0.15 g, 0.41 mmol), HOBt Hydrate (0.061 g, 0.45 mmol) and EDC hydrochloride (0.086 g, 0.45 mmol) in DCM (5 mL). After stirring at room temperature for 30 min, morpholine (0.04 mL, 0.45 mmol) was added. The reaction mixture was stirred at that temperature for 16 hours , washed firstly with 10% aqueous HCl, secondly with 10% aqueous $NaHCO_3$, and finally with 10% aqueous NaCl, dried over Na_2SO_4, filtered and concentrated, to give a residue which was purified by a flash chromatography on silica gel. Elution with 3/7 Cyclohexane/Ethyl Acetate gave 0.073 g (41%) of 2 as a white solid. mp: 268°C with partial decomposition. ^{1}H NMR (300 MHz, d_6-DMSO): δ 8.13 (bs, 1H), 7.86 (s, 1H), 7.29 (td, J = 9.4, 5.3 Hz, 1H), 7.08 (td, J = 9.0, 1.8 Hz, 1H), 6.92 (m, 3H), 4.64 (m, 1H), 4.47 (dd, J = 11.5, 2.3 Hz, 1H), 4.32 (m, 1H), 4.18 (dd, J = 11.5, 7.1 Hz, 1H), 4.02 (q, J = 7.2 Hz, 1H), 3.52 (d, J = 32.1 Hz, 10H) ppm. ^{13}C NMR (75 MHz, d_6-DMSO): δ 168.9, 161.8, 152.5 (dd, J = 240.3, 6.6 Hz), 148.3 (dd, J = 247.2, 8.5 Hz), 144.4, 143.1 (dd, J = 10.8, 3.1 Hz), 142.6, 129.2, 121.1, 117.4, 116.7, 117.0 (dd, J = 25.0, 20.2 Hz), 116.3 (d, J = 9.1 Hz), 111.5 (dd, J = 22.9, 3.9 Hz), 71.9, 68.6, 66.5, 65.0 ppm. Elemental analysis calculated (%) for ($C_{21}H_{20}F_2N_2O_6$): C 58.06; H 4.64; N 6.45. Found: C 57.90; H 4.70; N 6.40.

3-(benzyloxymethyl)-1,4-benzodioxan-6-carboxylic acid (16): A solution of **13** (10.31 g, 46.43 mmol) in dry THF (50) mL) was added to a suspension of NaH (2.78 g, 69.64 mmol) in THF (15 mL) at 0 °C. After stirring at room temperature for 30 minutes, benzyl bromide (8.28 mL, 69.64 mmol) was added. The reaction mixture was heated at reflux and stirred for 16 hours, concentrated under vacuum, diluted with MeOH (50 mL) and treated with 10% aqueous NaOH (36 mL, 90 mmol). The solution was heated at 50 °C, stirred for 2 hours, concentrated under vacuum, washed with Et_2O (30 mL), treated with concentrated HCl and finally extracted with Ethyl Acetate (3x25mL). The organic phase was dried over Na_2SO_4, filtered and concentrated under vacuum to give 12.76 g (91%) of **16** as a yellow oil. ^{1}H NMR (300 MHz, $CDCl_3$): δ 7.64 (m, 2H), 7.35 (m, 5H), 6.93 (dd, J = 8.7, 6.6 Hz, 1H), 4.61 (s, 2H), 4.38 (m, 2H), 4.16 (m, 1H), 3.77 (dd, J = 10.4, 4.8 Hz, 1H), 3.69 (dd, J = 10.4, 5.7 Hz, 1H) ppm.

3-(benzyloxymethyl)-1,4-benzodioxan-6-carboxamide (17): A solution of **16** (12.76 g, 42.49 mmol) in $SOCl_2$ (15.5 mL, 212.45 mmol) was stirred at 50 °C for 3 hours, concentrated under vacuum, diluted with DCM (100 mL), added with 30% aqueous NH_3 (25 mL) and stirred at room temperature for 24 hours. The reaction mixture was then concentrated, diluted with Ethyl Acetate, washed with 10% $NaHCO_3$ (2x15 mL), dried over Na_2SO_4, filtered and concentrated to give 11.06 g (87%) of **17** as a yellow oil. ^{1}H NMR (300 MHz, $CDCl_3$): δ 7.42–7.28 (m, 7H), 6.90 (d, J = 8.4 Hz, 1H), 4.60 (s, 2H), 4.35 (m, 2H), 4.12 (m, 1H), 3.75 (dd, J = 10.7, 4.9 Hz, 1H), 3.67 (dd, J = 10.7, 6.3 Hz, 1H) ppm.

3-(benzyloxymethyl)-1,4-benzodioxan-6-carbonitrile (18): Trifluoroacetic anhydride (22.62 mL, 162.74 mmol) was added to a solution of **17** (11.06g, 36.99 mmol) in dioxane/pyridine (4/1, 100 mL tot.) at 0 °C. The reaction mixture was stirred at room temperature for 16 hours, diluted with Ethyl Acetate (50 mL), washed firstly with 10% aqueous HCl (2x15 mL), secondly with 10% aqueous $NaHCO_3$ (15 mL), finally with 10% NaCl, dried over Na_2SO_4, filtered and concentrated under vacuum to give 8.32 g (80%) of **18** as a dark brown oil. ^{1}H NMR (300 MHz, $CDCl_3$): δ 7.42–7.28 (m, 5H), 7.17 (m, 2H), 6.92 (d, J = 8.3 Hz, 1H), 4.60 (s, 2H), 4.37 (m, 2H), 4.12 (m, 1H), 3.75 (dd, J = 10.4, 4.7 Hz, 1H), 3.67 (dd, J = 10.4, 5.6 Hz, 1H) ppm.

3-(hydroxymethyl)-1,4-benzodioxan-6-carbonitrile (19): Method C from **18** (3.72 g, 13.23 mmol), giving 2.47 g (quantitative) of **19** as a brown oil. ^{1}H NMR (300 MHz, $CDCl_3$): δ 7.17 (m, 2H), 6.94 (d, J = 8.3 Hz, 1H), 4.39 (dd, J = 11.2, 1.8 Hz, 1H), 4.27 (m, 1H), 4.18 (dd, J = 11.2, 7.8 Hz, 1H), 3.95 (dd, J = 12.1, 4.1 Hz, 1H), 3.87 (dd, J = 12.1, 4.8 Hz, 1H) ppm.

(7-cyano-1,4-benzodioxan-2-yl)methylmethansulfonate (20): Method A from **19** (2.47 g, 12.92 mmol), giving 3.30 g (95%) of **20** as a brown oil. ^{1}H NMR (300 MHz, $CDCl_3$): δ 7.20 (m, 2H), 6.97 (d, J = 8.8 Hz, 1H), 4.49 (m, 3H), 4.37 (dd, J = 10.6, 2.4 Hz, 1H), 4.18 (dd, J = 11.7, 6.7 Hz, 1H), 3.10 (s, 3H) ppm.

3-(7-cyano-1,4-benzodioxan-2-yl)methoxy-2,6-difluorobenzamide (21): Method B from **20** (0.89 g, 3.30 mmol), purifying the crude by flash chromatography on silica gel, eluting with 1/1 Cyclohexane/Ethyl Acetate and yielding 0.61 g (53%) of **21** as a white solid. mp: 158.2°C. ^{1}H NMR (300 MHz, d_6-DMSO): 8.10 (br s, 1H), 7.82 (br s, 1H), 7.40 (d, J = 1.9 Hz, 1H), 7.32 (dd, J = 8.4, 2.1 Hz, 1H), 7.26 (dt, J = 9.3, 5.1 Hz, 1H,), 7.07 (dt, J = 9.3, 2.0 Hz, 1H), 7.1 (d, J = 8.4 Hz, 1H,), 4.67 (m, 1H), 4.52 (dd, J = 11.6, 2.5 Hz, 1H), 4.27 (m, 3H) ppm.

3-(7-(1H-tetrazol-5-yl)-1,4-benzodioxan-2-yl)methoxy-2,6-difluorobenzamide (3): Sodium azide (0.19 g, 1.81 mmol) and ZnCl2 (0.13 g, 0.99 mmol) were added to a solution of 21 (0.2 g, 0.58 mmol) in 1/1 water/DMF (5 mL). The reaction mixture was stirred at 100 °C for 24 hours, concentrated under vacuum, diluted with Ethyl Acetate and treated with 10% $NaHCO_3$ (15 mL). The pH was brought to 1 treating with concentrated HCl and the aqueous phase was extracted with Ethyl Acetate (3x15 mL). The organic phase was dried over Na_2SO_4, filtered and concentrated under vacuum to give 0.1 g (44%) of 3 as a yellowish solid. mp = 198 °C. ^{1}H NMR (300 MHz, d_6-DMSO): δ 8.12 (bs, 1H), 7.85 (bs, 1H), 7.56 (m, 2H), 7.31 (dt, J = 9.0, 5.2 Hz, 1H), 7.14 (d, J = 9.0 Hz, 1H), 7.09 (dt, J = 9.0, 3.0 Hz, 1H), 4.76-4.62 (m, 1H), 4.53 (dd, J = 11.7, 2.5 Hz, 1H), 4.40 (dd, J = 11.0, 4.0 Hz, 1H), 4.34 (dd, J = 11.0, 5.8 Hz, 1H), 4.24 (dd, J = 11.5, 7.1 Hz, 1H) ppm. ^{13}C-NMR (75 MHz, d_6-DMSO): δ 161.7, 155, 152.6 (dd, J = 240.3, 6.7 Hz), 148.4 (dd, J = 247.4, 8.6 Hz), 145.8, 143.5, 143.1 (dd, J = 10.9, 3.2 Hz), 116.4 (d, J = 9.1 Hz), 116.2, 111.5 (dd, J = 22.8, 3.9 Hz), 71.9, 68.6, 65.1 ppm. Elemental analysis calculated (%) for ($C_{17}H_{13}F_2N_5O_4$): C, 52.45; H, 3.37; N, 17.99. Found: C, 52.39; H, 3.51; N, 17.68.

5-((3-benzyloxymethyl)-1,4-benzodioxan-6-yl)-1H-tetrazole (22). A solution of **18** (0.60 g, 2.11 mmol) in 1/1 water /DMF (10 mL) was added with sodium azide (0.43 g, 6.59 mmol) and ZnCl2 (0.49 g, 3.58 mmol), at room temperature. The reaction was then heated to 100 °C and left stirring for 16 hours. At completion, the mixture was then concentrated under reduced pressure, resumed with Ethyl Acetate (20 mL) and washed with aqueous 10% NaCl (3 x 15 mL); the organic layer was then dried over Na_2SO_4, filtered and concentrated under reduced pressure, accomplishing 650 mg (95%) of **22** as a brownish oil. ^{1}H NMR (300 MHz, $CDCl_3$): δ= 7.51 (m, 2H), 7.37-7.31 (m, 5H), 6.97 (d, J = 8.63 Hz, 1H), 4.62 (s, 2H), 4.42-4.29 (m, 2H), 4.15 (dd, J = 10.6, 7.1 Hz, 1H), 3.75 (dd, J = 10.6, 5.3 Hz, 2H) ppm.

5-((3-benzyloxymethyl)-1,4-benzodioxan-6-yl)-1-methyl-tetrazole (23) and 5-((3-benzyloxymethyl)-1,4-benzodioxan-6-yl)-2-methyl-tetrazole (24). Method D from **22** (0.65 g, 2.00 mmol) in DMF and stirring for 3 hours. Purification by flash chromatography on silica gel, eluting with 7/3 Cyclohexane/Ethyl Acetate, yielded 120 mg of **23** as white wax and 380 mg of **24** as light yellow oil. Cumulative yield: 77.3%. 5-((3-benzyloxymethyl)-1,4-benzodioxan-6-yl)-1-methyl-tetrazole (**23**): ^{1}H NMR (300 MHz, $CDCl_3$): δ= 7.34 (m, 5H), 7.28 (m, 2H), 7.04 (d, J = 8.3 Hz, 1H), 4.62 (s, 2H), 4.36 (m, 2H), 4.18 (dd, J = 10.4, 7.6 Hz, 1H), 4.15 (s, 3H), 3.78 (dd, J = 10.4, 4.8 Hz, 1H), 3.70 ppm (dd, J = 10.4, 5.5 Hz, 1H). 5-((3-benzyloxymethyl)-1,4-benzodioxan-6-yl)-2-methyl-tetrazole (**24**): ^{1}H NMR (300 MHz, $CDCl_3$): δ= 7.64 (m, 2H), 7.35-7.29 (m, 5H), 6.98 (d, J = 8.2 Hz, 1H), 4.62 (s, 2H), 4.45-4.33 (m, 2H), 4.37 (s, 3H), 4.16 (dd, J = 10.3, 7.1 Hz, 1H), 3.78 (dd, J = 10.4, 4.3 Hz, 1H), 3.70 (dd, J = 10.4, 5.8 Hz, 1H) ppm.

5-((3-hydroxymethyl)-1,4-benzodioxan-6-yl)-1-methyl-tetrazole (25): Method C from 23 (0.38 g, 0.98 mmol), giving 190 mg (99.2%) of 25 as a yellowish oil. ^{1}H NMR (300 MHz, $CDCl_3$): δ= 7.35 (m, 2H), 7.06 (d, J = 8.4 Hz, 1H), 4.36 (m, 2H), 4.17 (dd, J = 12.7, 7.5 Hz, 1H), 4.17 (s, 3H), 3.97 (dd, J = 12.1, 4.2 Hz, 1H), 3.89 ppm (dd, J = 12.1, 4.9 Hz, 1H).

5-((3-hydroxymethyl)-1,4-benzodioxan-6-yl)-2-methyl-tetrazole (26): Method C from **24** (0.12 g, 0.31 mmol), giving 50 mg (99%) of **26** as a yellowish oil. ^{1}H NMR (300 MHz, $CDCl_3$): δ= 7.69 (d, J = 2.0 Hz, 1H), 7.63 (dd, J = 8.4, 2.0 Hz, 1H), 6.99 (d, J = 8.4 Hz, 1H), 4.32 (m, 2H), 4.37 (s, 3H), 4.18 (dd, J = 10.9, 7.3 Hz, 1H), 3.95 (dd, J = 12.0, 4.2 Hz, 1H), 3.87 (dd, J = 12.0, 5.0 Hz, 1H) ppm.

5-((3-mesyloxymethyl)-1,4-benzodioxan-6-yl)-1-methyl-tetrazole (27): Method A from **25** (0.19 g, 0.97 mmol), giving 200 mg (83.3%) of **27** as a brown oil. ^{1}H NMR (300 MHz, $CDCl_3$): δ= 7.31 (m, 2H), 7.08 (d, J = 8.4 Hz, 1H), 4.55 (m, 1H), 4.47 (m, 2H), 4.41 (m, 1H), 4.22 (dd, J = 11.7, 7.5 Hz, 1H), 4.17 (s, 3H), 3.11 (s, 3H) ppm.

5-((3-mesyloxymethyl)-1,4-benzodioxan-6-yl)-2-methyl-tetrazole (28): Method A from **26** (0.05 g, 0.28 mmol), giving 60 mg (83%) of **28** as a yellow oil. ^{1}H NMR (300 MHz, $CDCl_3$): δ= 7.67 (m, 1H), 7.36 (m, 1H), 6.98 (d, J= 8.4 Hz, 1H), 4.85 (m, 2H), 4.36 (m, 2H), 4.37 (s, 3H), 4.18 (dd, J = 11.4, 6.4 Hz, 1H), 3.11 (s, 3H) ppm.

3-(7-(1-methyl-tetrazol-5-yl)-1,4-benzodioxan-2-yl)methoxy-2,6-difluorobenzamide (4): Method B from **27** (0.20 g, 0.19 mmol), purifying the crude by crystallization from chloroform and yielding 170 mg (62.5%) of **4** as a white solid. mp: 190-192 °C. ^{1}H NMR (300 MHz, DMSO-d_6) δ= 8.09 (bs, 1H), 7.81 (bs, 1H), 7.38 (d, J = 2.1 Hz, 1H), 7.32 (dt, J = 8.4, 2.1 Hz, 1H), 7.26 (d, J = 9.0 Hz, 1H), 7.11 (d, J = 8.4 Hz, 1H), 7.05 (dt, J = 9.0, 2.0 Hz, 1H), 4.67 (m, 1H), 4.52 (dd, J = 11.6, 2.4 Hz, 1H), 4.34 (dd, J = 28.5, 4.8 Hz, 1H), 4.34 (dd, J = 11.1, 4.8 Hz, 1H), 4.22 (dd, J = 11.6, 7.2 Hz, 1H), 4.10 (s, 3H) ppm. ^{13}C NMR (75 MHz, DMSO-d_6): δ= 161.6, 153.9, 152.6 (dd, J = 240.2, 6.8 Hz), 148.4 (dd, J = 247.3, 8.5 Hz), 145.6, 143.3, 143.1 (dd, J = 10.8, 3.1 Hz), 122.7 (d, J = 9.1 Hz), 118.3, 117.3, 117.1 (dd, J = 24.8, 20.6 Hz), 116.3 (dd, J = 9.2, 2 Hz), 111.5 (dd, J = 22.8, 3.9 Hz), 72, 68.6, 65.1, 35.4 ppm. Elemental analysis calculated (%) for ($C_{18}H_{15}F_2N_5O_4$): C, 53.60; H, 3.75; N, 17.36. Found: C, 53.41; H, 3.91; N, 17.20.

3-(7-(2-methyl-tetrazol-5-yl)-1,4-benzodioxan-2-yl)methoxy-2,6-difluorobenzamide (5): Method B from **28** (0.06 g, 0.23 mmol), purifying the crude by flash chromatography on silica gel, eluting with Cyclohexane/Ethyl Acetate 7/3 and affording 33 mg (37.4%) of **5** as a white solid. mp: 187 °C. ^{1}H NMR (300 MHz, DMSO-d_6) δ= 8.11 (bs, 1H), 7.83 (bs, 1H), 7.53 (td, J = 8.4, 2.1 Hz, 2H), 7.32 (dt, J = 9.3, 5.2 Hz, 1H), 7.08 (td, J = 9.1, 1.9 Hz, 1H), 7.08 (d, J = 8.4 Hz, 1H), 4.67 (m, 1H), 4.51 (dd, J = 11.6, 2.4 Hz, 1H), 4.35 (m, 2H), 4.39 (s, 3H), 4.23 (dd, J = 11.6, 7.1 Hz, 1H) ppm. ^{13}C NMR (75 MHz, DMSO-d_6): δ= 164.1, 161.7, 152.6 (dd, J = 240.3, 6.7 Hz), 148.4 (dd, J = 247.3, 8.4 Hz), 145.2, 143.4, 143.1 (dd, J = 10.8, 3.3 Hz), 121, 120.2, 117.1 (dd, J = 24.8, 20.3 Hz), 116.4 (d, J = 7.2 Hz), 115.3 (dd, J = 22.9, 3.9 Hz), 71.9, 68.6, 65.1, 40.0 ppm. Elemental analysis calculated (%) for ($C_{18}H_{15}F_2N_5O_4$): C, 53.60; H, 3.75; N, 17.36. Found: C, 53.50; H, 3.87; N, 17.12;

2,6-difluoro-3-(7-(N'-hydroxycarbamimidoyl)-1,4-benzodioxan-2-yl)methoxybenzamide (29): A solution of potassium Carbonate (2.55 g, 18.48 mmol) in H_2O (5 mL) was added to a solution of **21** (1.28 g, 3.70 mmol) and Hydroxylamine hydrochloride (1.28 g, 18.48 mmol) in ethanol (45 mL). The reaction mixture was stirred at reflux for 18 hours, concentrated under vacuum, diluted with Et_2O (10 mL) and extracted with 10% aqueous HCl (2x10mL). The aqueous phase was neutralized with 10% aqueous $NaHCO_3$ and extracted with Ethyl Acetate (3x10 mL). The organic phase was dried over Na_2SO_4, filtered and concentrated under vacuum to give 1.20 g (85%) of **29** as a brown oil. ^{1}H NMR (300 MHz, DMSO-d_6) δ= 9.49 (s, 1H), 8.12 (bs, 1H), 7.85 (bs, 1H), 7.30 (m, 1H), 7.18 (m, 2H), 7.07 (dt, J = 9.1, 1.9 Hz, 1H), 6.87 (d, J = 8.1 Hz, 1H), 4.58 (m, 1H), 4.43 (dd, J = 11.3, 2.4 Hz, 1H), 4.32 (m, 2H), 4.13 (dd, J = 11.3, 7.1 Hz, 1H) ppm.

2,6-difluoro-7-((1,2,4-oxadiazol-5-one-3-yl)-1,4-benzodioxan-2-yl)methoxybenzamide (6): DBU (0.13 mL, 0.86 mmol) and CDI (0.14 g, 0.86 mmol) were added to a solution of **29** (0.25 g, 0.66 mmol) in dioxane (10 mL). The reaction mixture was stirred at reflux for 18 hours, diluted with DCM (15 mL), washed with 10% aqueous HCl (2x5 mL), dried over Na_2SO_4, filtered and concentrated under vacuum. The residue was purified by crystallization from DCM/Ethyl Acetate 1/3 to give 21o mg (79%) of **6** as a white solid. mp: 250 °C ^{1}H NMR (300 MHz, DMSO-d_6): δ= 12.79 (s, 1H), 8.12 (bs, 1H), 7.85 (bs, 1H), 7.30 (m, 3H), 7.05 (m, 1H), 7.08 (d, J = 9 Hz, 1H), 4.67 (m, 1H), 4.51 (dd, J = 11.7, 2.4 Hz, 1H), 4.46 (m, 2H), 4.21 (dd, J = 11.6, 7.2 Hz, 1H) ppm. ^{13}C NMR (75 MHz, DMSO-d_6): δ= 161.7, 160.4, 157.3, 152.6 (dd, J = 240.2, 6.8 Hz), 148.3 (dd, J = 247.3, 8.6 Hz), 146.5, 143.3, 143.1 (dd, J = 11.0, 3.3 Hz), 120.0, 118.5, 117.0 (dd, J = 25.0, 20.4 Hz), 116.9, 116.3 (dd, J = 9.1, 1.5 Hz), 115.5, 111.5 (dd, J = 22.8, 4.0 Hz), 71.9, 68.5, 65.1 ppm. Elemental analysis calculated (%) for ($C_{18}H_{13}F_2N_3O_6$): C, 53.34; H, 3.23; N, 10.37. Found: C, 53.31; H, 3.28; N, 10.31.

2,6-difluoro-7-((N'-methyl-1,2,4-oxadiazol-5-one-3-yl)-1,4-benzodioxan-2-yl)methoxybenzamide (7): Method D from **6** (0.15 g, 0.38 mmol) in ACN and stirring for 18 hours. Purification by flash chromatography on silica gel, eluting with 7/3 Cyclohexane/Ethyl Acetate, yielded 70 mg of **7** as a white solid. mp: 230 °C with partial decomposition. ^{1}H NMR (300 MHz, DMSO-d_6): δ= 8.11 (bs, 1H), 7.84 (bs, 1H), 7.28 (m, 3H), 7.12 (m, 2H), 4.69 (m, 1H), 4.54 (dd, J = 11.6, 2.3 Hz, 1H), 4.37 (m, 2H), 4.24 (dd, J = 11.6, 7.1 Hz, 1H), 3.18 (s, 3H) ppm. ^{13}C NMR (75 MHz, DMSO-d_6): δ= 161.9, 159.8, 159.0, 152.6 (dd, J = 240.0, 6.8 Hz), 148.4 (dd, J = 247.1, 8.6 Hz), 146.3, 143.3, 143.1 (dd, J = 10.5, 3.0 Hz), 122.4, 118.4, 117.7, 116.9 (dd, J = 24.8, 19.5 Hz), 116.6, 116.5 (dd, J = 9.8, 1.5 Hz), 111.5 (dd, J = 22.9, 4.1 Hz), 72.0, 68.6, 65.1, 29.9 ppm. Elemental analysis calculated (%) for ($C_{19}H_{15}F_2N_3O_6$): C, 54.42; H, 3.61; N, 10.02. Found: C, 54.22; H, 3.84; N, 9.92.

2,6-difluoro-7-((5-mercapto-1,2,4-oxadiazol-3-yl)-1,4-benzodioxan-2-yl)methoxybenzamide (8): DBU (0.20 mL, 1.37 mmol) and TCDI (0.24 g, 1.37 mmol) were added to a solution of **29** (0.4 g, 1.05 mmol) in ACN (10 mL). The reaction mixture was stirred at reflux for 18 hours, diluted with DCM (15 mL), washed with 10% aqueous HCl (2x5 mL), dried over Na_2SO_4, filtered and concentrated under vacuum. The residue was purified by crystallization from Ethyl Acetate to give 0.1 g (23%) of **8** as a yellow solid. mp= 173 °C with decomposition. ^{1}H NMR (300 MHz, DMSO-d_6): δ= 8.14 (bs, 1H), 7.87 (bs, 1H), 7.43 (m, 2H), 7.31 (td, J = 9.3, 5.2 Hz, 1H), 7.09 (m, 2H), 4.69 (m, 1H), 4.54 (dd, J = 11.6, 2.3 Hz, 1H), 4.39 (dd, J = 11.1, 3.8 Hz, 1H), 4.33 (dd, J = 11.1, 5.7 Hz, 1H), 4.24 (dd, J = 11.6, 7.1 Hz, 1H) ppm. ^{13}C NMR (75 MHz, DMSO-d_6): δ= 188.2, 161.9, 159.6, 152.6 (dd, J = 240.8, 6.8 Hz), 148.4 (dd, J = 247.5, 8.2 Hz), 146.7, 143.4, 143.1 (dd, J = 10.9, 3.4 Hz), 120.9, 118.6, 116.9 (dd, J = 24.7, 20.2 Hz), 116.5 (dd, J = 9.0, 2.3 Hz), 116.2, 115.8, 111.5 (dd, J = 23.3, 3.7 Hz), 71.9, 68.6, 65.1 ppm. Elemental analysis calculated (%) for ($C_{18}H_{13}F_2N_3O_5S$): C, 51.31; H, 3.11; N, 9.97. Found: C, 51.01; H, 3.28; N, 9.87.

2,6-difluoro-7-((5-methylthio-1,2,4-oxadiazol-3-yl)-1,4-benzodioxan-2-yl)methoxybenzamide (9): Method D from 8 (0.14 g, 0.33 mmol) in ACN and stirring for 18 hours. Purification by flash chromatography on silica gel, eluting with 7/3 Cyclohexane/Ethyl Acetate, yielded 70 mg of 9 as a white solid. mp: 165 °C. ^{1}H NMR (300 MHz, DMSO-d_6): δ= 8.12 (bs,

1H), 7.84 (bs, 1H), 7.49 (dd, J = 8.4, 2.0 Hz, 1H), 7.45 (m, 1H), 7.31 (dt, J = 9.3, 5.3 Hz, 1H), 7.08 (d, J = 8.4 Hz, 1H), 7.08 (dt, J = 8.9, 1.8 Hz, 1H), 4.68 (m, 1H), 4.52 (dd, J = 11.6, 2.3 Hz, 1H), 4.38 (dd, J = 11.2, 4.2 Hz, 1H), 4.33 (dd, J = 11.2, 5.8 Hz, 1H), 4.24 (dd, J = 11.6, 7.2 Hz, 1H), 2.80 (s, 3H) ppm. ^{13}C NMR (75 MHz, DMSO-d_6): δ= 179.0, 167.8, 161.7, 152.6 (dd, J = 240.8, 6.8 Hz), 148.4 (dd, J = 247.1, 8.6 Hz), 146.2, 143.4, 143.1 (dd, J = 11.2, 3.0 Hz), 121.1, 119.6, 118.4, 117.1 (dd, J = 24.7, 20.2 Hz), 116.4 (dd, J = 9.4, 1.9 Hz), 116.2, 111.5 (dd, J = 22.5, 3.7 Hz), 71.9, 68.6, 65.2, 15.1 ppm. Anal. Calcd for ($C_{19}H_{15}F_2N_3O_5S$): C, 52.41; H, 3.47; N, 9.65. Found: C, 52.39; H, 3.48; N, 9.64.

2,6-difluoro-7-((5-methyl-1,2,4-oxadiazol-3-yl)-1,4-benzodioxan-2-yl)methoxybenzamide (10): Acetic anhydride (0.1 mL, 1.05 mmol) was added to a solution of 29 (0.4 g, 1.05 mmol) in DCM/DMF (10 mL + 2 mL). The reaction mixture was stirred at room temperature for 2 hours, diluted with DCM, washed with 10% aqueous $NaHCO_3$, dried over Na_2SO_4, filtered and concentrated under vacuum. The residue was diluted with DMF (5 mL), added with NaOH (0.2 g, 5 mmol) and stirred for 18 hours. The reaction mixture was then diluted with H_2O and filtered to give a solid. The residue was purified crystallizing from ethanol, obtaining 40 mg (9%) of 10 as a white solid. mp: 155 °C. ^{1}H NMR (300 MHz, DMSO-d_6): δ= 8.14 (bs, 1H), 7.86 (bs, 1H), 7.50 (dd, J = 8.4, 2.0 Hz, 1H), 7.45 (dd, J = 4.8, 2.0 Hz, 1H), 7.31 (dt, J = 9.5, 3.9 Hz, 1H), 7.09 (m, 1H), 7.07 (dd, J = 8.4, 4.8 Hz, 1H), 4.68 (m, 1H), 4.51 (ddd, J = 11.6, 4.5, 2.5 Hz, 1H), 4.39 (dd, J = 11.5, 4.5 Hz, 1H), 4.33 (dd, J = 11.5, 5.9 Hz, 1H), 4.23 (dd, J = 11.6, 7.0 Hz, 1H), 2.63 (s, 3H) ppm. ^{13}C NMR (75 MHz, DMSO-d6): δ= 177.7, 167.5, 161.7, 152.6 (dd, J = 240.0, 6.8 Hz), 148.4 (dd, J = 247.5, 8.3 Hz), 143.3, 143.1 (dd, J = 10.9, 3.4 Hz), 121.0, 120.2, 118.4, 117.1 (dd, J = 24.8, 20.3 Hz), 116.4 (dd, J = 9.4, 1.9 Hz), 116.0, 111.5 (dd, J = 22.9, 4.1 Hz), 71.9, 68.6, 65.1, 12.5 ppm. Elemental analysis calculated (%) for ($C_{19}H_{15}F_2N_3O_5$): C, 56.58; H, 3.75; N, 10.42; Found: C, 56.49; H, 3.83; N, 10.34.

2,6-difluoro-7-((5-ethyl-1,2,4-oxadiazol-3-yl)-1,4-benzodioxan-2-yl)methoxybenzamide (11): Propionic anhydride (0.12 mL, 0.9 mmol) was added to a solution of 29 (0.34 g, 0.9 mmol) in DCM/DMF (10 mL + 2 mL). The reaction mixture was stirred at room temperature for 2 hours, diluted with DCM, washed with 10% aqueous $NaHCO_3$, dried over Na_2SO_4, filtered and concentrated under vacuum. The residue was diluted with DMF (5 mL), added NaOH (0.2 g, 5 mmol), stirred for 18 hours, concentrated under vacuum, diluted with Ethyl Acetate (10 mL), washed with 10% aqueous NaCl (3x5 mL), dried over Na_2SO_4, filtered and concentrated to give a residue which was purified by flash chromatography on silica gel. Elution with 3/7 Cyclohexane/Ethyl Acetate gave 0.14 g (37%) of 10 as a white solid. mp: 164 °C ^{1}H NMR (300 MHz, DMSO-d_6): δ= 8.14 (bs, 1H), 7.87 (bs, 1H), 7.51 (dd, J = 8.4, 1.9 Hz, 1H), 7.46 (m, 1H), 7.32 (dt, J = 9.4, 5.3 Hz, 1H), 7.10 (m, 1H), 7.08 (dd, J = 8.4, 1H), 4.68 (m, 1H), 4.52 (dd, J = 11.6, 2.3 Hz, 1H), 4.39 (dd, J = 11.2, 4.5 Hz, 1H), 4.33 (dd, J = 11.2, 5.8 Hz, 1H), 4.24 (dd, J = 11.6, 7.1 Hz, 1H) ,2.98 (q, J = 7.6 Hz, 2H), 1.32 (t, J = 7.6 Hz, 3H) ppm. ^{13}C NMR (75 MHz, DMSO-d6): = 181.4, 167.4, 161.7, 152.6 (dd, J = 240.0, 6.8 Hz), 148.4 (dd, J = 247.1, 8.6 Hz), 146.0, 143.3, 143.1 (dd, J = 10.5, 3.0 Hz), 121.0, 120.2, 118.3, 117.1 (dd, J = 25.1, 19.9 Hz), 116.3, 116.0 (d, J = 14.6 Hz), 111.5 (dd, J = 23.6, 2.6 Hz), 71.9, 68.6, 65.1, 20.0, 10.9 ppm. Elemental analysis calculated (%) for ($C_{20}H_{17}F_2N_3O_5$): C, 57.56; H, 4.11; N, 10.07. Found: C, 57.55; H, 4.11; N, 10.04.

Cells

Normal human lung fibroblasts (MRC-5) were grown in Dulbecco's modified Eagle's medium (DMEM) supplemented with 10% heat-inactivated calf serum, 100 U/mL penicillin and 100 mg/mL streptomycin in an incubator at 5% CO_2 atmosphere and 37 °C. The Gram-positive *Staphylococcus aureus* (methicillin-sensitive MSSA ATCC 29213, and methicillin-resistant MRSA ATCC 43300) and the Gram-negative *Escherichia coli* (ESBL, extended-spectrum beta-lactamase-positive E. coli) bacterial cells were grown in Luria-Bertani Broth (LB) medium at 37 °C under constant shaking at 300 rpm.

Optical microscopy

Cells were grown over night in the presence of increasing concentrations of the compounds showing an evident inhibitory activity at concentrations lower than 1 µg/ml, starting from the previously determined MIC. Data are reported for *S. aureus* cultured in the presence of **9** (0.6 µg/ml) and DFNB (0.25 µg/ml) as a positive control. Untreated *S. aureus* cultures were used as negative control. Samples were analysed by phase contrast under a Zeiss Axioskop microscope.

Transmission electron microscopy

S. aureus (10^9 cells/ml) were cultured in the presence of 9 and DFNB (positive control), at the same concentrations used for optical microscopy and, after 16 hours incubation at 37 °C, the cells were harvested and processed for transmission electron microscopy, as already described [37]. Untreated *S. aureus* was used as negative control. After centrifugation at 3100 x g for 5 min at room temperature, pelleted bacteria were fixed in 2.5% glutaraldehyde (Polysciences, Warrington, PA) in 0.1 M Na cacodylate buffer, pH 7.4, for 1 h at 4 °C, rinsed twice, and post-fixed in Na cacodylate-buffered 1% OsO_4, for 1 h at 4 °C. The samples were dehydrated through a series of graded ethanol solutions and propylene oxide and embedded in Poly/Bed 812 resin mixture. Ultrathin sections were obtained using a Reichert-Jung ultramicrotome equipped with a diamond knife. Samples were then stained with water-saturated uranyl acetate and 0.4% lead citrate in 0.1 M NaOH. The specimens were viewed under a Philips CM10 electron microscope.

Antibacterial activity

The antibacterial activity of compounds **1-11** and **III**-**V** was tested by using both a methicillin-sensitive and a methicillin-resistant *S. aureus* strain, and an ESBL *E. coli* clinical isolate. All of the compounds were dissolved at the final concentration of 20 mg/mL in dimethyl sulphoxide (DMSO) and serially diluted in LB. After incubation at 37 °C for 16 hours in aerobic culture tubes, the concentration of prokaryotic cells was determined by optical density measurement, at 600 nm (OD600) in a SmartSpec™ 3000 spectrophotometer (Bio-Rad, Oceanside, CA, USA). Fresh cell cultures were used at 10^5 cells/mL in a final volume of 2 mL. Each bacterial sample was grown with different compound concentrations that ranged from 100 to 0.1 µg/mL for the first screening of all the compounds.

For compounds **4**, **9**, **10** and **11**, that were active up to 10 µg/mL but not at 0.1 µg/mL further analyses with intermediate concentrations were performed. After incubation of each sample overnight at 37 °C, an aliquot was collected under sterile conditions and the OD600 was measured to determine the MIC. To determine the MBC, the bacteria were then washed three times with LB, centrifuged at 900× g for 10 min at 4 °C, and the pellet resuspended in fresh LB. After overnight incubation at 37 °C, the absence of growth was confirmed by OD measurement. All tests were performed in triplicate and for each series of experiments, both positive (no compounds) and negative (no bacteria) controls were included.

Antimicrobial activities of compounds against MRSA 11.7, MRSA 12.1 and mutated *E. coli* were determined by the broth microdilution method in 96-well plate format following the Clinical and Laboratory Standards Institute (CLSI) guidelines and European Committee on Antimicrobial Susceptibility Testing (EUCAST) recommendations. Bacterial suspension of specific bacterial strain equivalent to 0.5 McFarland turbidity standard was diluted with cation-adjusted Mueller Hinton broth with TES (Thermo Fisher Scientific), to obtain a final inoculum of 10^5 CFU/ml. Compounds dissolved in DMSO and inoculum were mixed together and incubated for 20 h at 37 °C. After incubation the minimal inhibitory concentration (MIC) values were determined by visual inspection as the lowest dilution of compounds showing no turbidity. Tetracycline was used as a positive control on every assay plate.

Thiazolyl blue tetrazolium bromide cytotoxicity assay

Compounds **4**, **9**, **10** and **11**, showing an antibacterial activity at a concentration lower than 10 µg/ml, were serially diluted in DMEM and tested on MRC-5 cells by the thiazolyl blue tetrazolium bromide (MTT) cytotoxicity assay (Sigma, St Louis, MO, USA). Cells (10^4 cell/well) were tested in a 96-well plate using serially two-fold-diluted concentrations of

the compound in 100 µl DMEM medium. After a 24-h incubation, the compound was removed and the cells were overlaid with 1 mg/ml MTT in 100 µl serum-free DMEM for 3 h at 37 °C. The MTT solution was then replaced with DMSO for 10 min, and the absorbance was measured at 570 nm. The percentage of cytotoxicity was calculated by the formula 100 – (sample OD/untreated cells OD) x 100. The compound concentration reducing cell viability by 50 or 90% was defined as the TD50 or TD90 toxic dose. The therapeutic index (TI) was also determined and defined as the ratio between TD90 and the minimal bactericidal concentration (MBC) values.

Computational studies

Ligand preparation. The preparation of the compounds synthesized in this work was performed before carrying out further computational studies. The preparation together with the 2D-to-3D conversion was performed using LigPrep tool, [38] that is included in the Schrödinger software package. This application allows the preparation of molecules following different steps required for ligand-protein analysis such as the addition of hydrogen atoms, the calculation of the ionization state of the molecules at a specific pH or the generation of potential tautomers. Also, low-energy ring conformations are generated for every molecule, followed by a final energy minimization using the OPLS-2005 force field. [39,40] In order to perform the studies, physiological pH conditions were used to prepare the molecules, all of them were desalted and in the last step the compounds were minimized as default.

Protein preparation. In order to obtain the crystal structure of the protein to carry out the computational studies, a search on the PDB [41] was performed. According to the crystal structures available in the PDB of the FtsZ protein from *S. aureus*, two entries were retrieved: 4DXD [14] and 5XDT [22]. The selection was based on the experimental quality of the structure and the presence of a ligand in the active site. In this case, both crystals are holo structures with a potent inhibitor bound to the protein. These inhibitors displayed a 2,6-difluorobenzamide scaffold identical to one of the moieties that is present in the family of inhibitors described here. The structures of the proteins were preprocessed adding the corresponding hydrogens, deleting water molecules and assigning bond orders. Also the proteins were refined carrying out H-bond assignment and calculation of the protonation state of the residues at physiological pH with a final restraint minimization, using the Protein Preparation Wizard tool [42] implemented on Maestro software. [43]

Ligand Characterization. The compounds previously prepared were analyzed using the Qikprop [35] module of the small molecule drug discovery suite in the Schrödinger software package. Among other parameters, ADME Tox properties were predicted using the Qikprop program. Qikprop allowed us to calculate and predict a total of 44 pharmaceutical relevant properties. These properties include both simple molecular descriptors and relevant computational predictions for drug discovery. Among other parameters it is possible to calculate the following descriptors: molecular weight (MW), molecular volume, number of hydrogen bond acceptor and donor (HBA, and HBAs respectively), PSA, QPlogPo/w (predicted octanol/water partition coefficient), dipole values and violations related to Lipinski's rule of five [44] and Jorgensen's rule of three. [45]

Docking studies. Docking studies were performed employing Glide module [46] included in the Schrödinger software package. As a first approach, docking studies with the previously crystallized ligands were performed to validate the protocol. Once, the protocol was validated. The selected 3D target structures of FtsZ from *S. aureus* and the compounds synthesized in this work were used as a starting point of the analysis. Docking studies were carried out applying a similar protocol in terms of conformational search and evaluation parameters for all the compounds. In all the cases, the center of the previously crystallized ligand in the catalytic pocket was selected as the centroid of the grid. In the grid generation, a scaling factor of 1.0 in van der Waals radius scaling and a partial charge cutoff of 0.25 were used. The xtra precision (XP) mode was used in the docking studies for all the molecules and no constraints were applied during the process. The ligand sampling was flexible, epik state penalties were added to the docking score and an energy window of 2.5 kcal/mol was used for ring sampling. In the energy minimization step, distance dependent dielectric constant was 4.0 with a maximum number of minimization steps of 100,000. In the clustering, poses were considered as duplicates and discarded if both: RMS deviation is less than 0.5 Å and maximum atomic displacement is less than 1.3 Å.

Hotspots maps. The Fragment Hotspot maps software [36] identifies the location and environment of binding sites on the protein by first calculating atomic hotspots and then producing Fragment Hotspot maps using simple molecular probes. These maps specifically highlight fragment-binding sites and their corresponding pharmacophores. H-Bond acceptor (red), donor (blue), and apolar/aromatic interactions (yellow), identified by this tool, can assist medicinal chemists in the search of interesting interactions. In this sense, it allows predicting the bind or improve the binding affinities for different ligands, and suggest modifications to the molecules. In this work, the structure of FtsZ from *S. aureus* was analyzed according the hotspots maps with the objective of obtaining more insights of the binding pocket in the protein. Also, the full structure of the protein was inspected in order to identify potential alternative or allosteric pockets useful in future drug discovery programs.

Induced Fit Docking. This study is carried out by fitting the ligand to the protein and permitting changes in the active site geometry. [47,48] This was done by docking the compound **9**, the reference compound in the study, to the protein in the Glide program [49,50] and generating several poses in the active site. Then, Prime [51] predicts the protein structure using the pose of the corresponding ligand and rearranging nearby side chains of the active site and minimizing the overall energy of the protein. [49, 52] Finally, each ligand is re-docked into its corresponding low energy protein structures and the resulting complexes are ranked according to docking score. No constraints were set, XP (extra precision) mode was used in a standard protocol, the induced fit was optimized to 5.0 Å of the ligand poses and the rest of the parameters were set to default.

Keywords: FtsZ inhibition; 1,4-benzodioxane-2,6-difluorobenzamide; Mutated E. coli; Molecular Modelling; Cavity Detection

References:

[1] González-Bello, C. Recently developed synthetic compounds with anti-infective activity. *Current Opinion in Pharmacology* **2019**, *48,* 17-23.

[2] Solomon, S. L.; Oliver, K. B. Antibiotic Resistance Threats in the United States: Stepping Back from the Brink. *American Family Physician* **2014** *89*, 938-941.

[3] Li, Y.; Yang, L.; Fu, J.; Yan, M.; Chen, D.; Zhang, L. Microbial pathogenicity and virulence mediated by integrons on Gram-positive microorganisms. *Microbial Pathogenesis* **2017**, *111*, 481-486.

[4] McGuinness, W. A.; Malachowa, N.; DeLeo, F. R. Vancomycin Resistance in Staphylococcus aureus. *Yale journal of Biology and Medicine*, **2017**, 269-281.

[5] Foster, T. J. Antibiotic resistance in Staphylococcus aureus. Current status and future prospects. *FEMS Microbiology Reviews* **2017**, *41*, 430-449.

[6] Rengaraj, R.; Mariappan, S.; Sekar, U.; Kamalanadhan, A. n. Detection of Vancomycin Resistance among Enterococcus faecalis and Staphylococcus aureus. *Journal of Clinical and Diagnostic Research* **2016**, *10*, DC04-DC06.

[7] Brauers, J.; Ewig, S.; Kresken, M. β-Lactam-Antibiotika in der Therapie von ambulant erworbenen Atemwegsinfektionen mit Penicillin-resistenten Pneumokokken. *Pneumologie* **2002**, *56*, 605-609.

[8] Saenz, Y.; Brinas, L.; Domínguez, E.; Ruiz, J.; Zarazaga, M.; Vila, J.; Torres, C. Mechanisms of Resistance in Multiple-Antibiotic-Resistant Escherichia coli Strains of Human, Animal, and Food Origins. *Antimicrobial Agents and Chemotherapy* **2004**, *48*, 3996-4001.

[9] Panda, D.; Bhattacharya, D.; Gao, Q. H.; Oza, P. M.; Lin, H.-Y. J.; Hawkins, B.; Hibbs, D. E.; Groundwater, P. W. Identification of agents

targeting FtsZ assembly. *Future Medicinal Chemistry* **2016**, *8*, 1111-1132.

[10] Vaughan, S.; Wickstead, B.; Gull, K.; Addinall, S. G. Molecular Evolution of FtsZ Protein Sequences Encoded Within the Genomes of Archaea, Bacteria, and Eukaryota. *Journal of Molecular Evolution* **2004**, *58*, 19-29.

[11] Haydon, D. J.; Stokes, N. R.; Ure, R.; Galbraith, G.; Bennett, J. M.; Brown, D. R.; Patrick J. Baker; Barynin, V. V.; Rice, D. W.; Sedelnikova, S. E.; Heal, J. R.; Sheridan, J. M.; Aiwale, S. T.; Chauhan, P. K.; Srivastava, A.; Taneja, A.; Collins, I.; Errington, J.; Czaplewski, L. G. An Inhibitor of FtsZ with Potent and Selective Anti-Staphylococcal Activity. *Science* **2008**, *321*, 1673-1675.

[12] Kaul, M.; Mark, L.; Zhang, Y.; Parhi, A. K.; LaVoie, E. J.; Pilch, D. S. Pharmacokinetics and in vivo antistaphylococcal efficacy of TXY541, a 1-methylpiperidine-4-carboxamide prodrug of PC190723. *Biochemical Pharmacology* **2013**, *86*, 1699-1707.

[13] Kaul, M.; Mark, L.; Zhang, Y.; Parhi, A. K.; Lyu, Y. L.; Pawlak, J.; Saravolatz, S.; Saravolatz, L. D.; Weinstein, M. P.; LaVoie, E. J.; Pilch, D. S. TXA709, an FtsZ-Targeting Benzamide Prodrug with Improved Pharmacokinetics and Enhanced In Vivo Efficacy against Methicillin-Resistant Staphylococcus aureus. *Antimicrobial Agents and Chemotherapy* **2015**, *59*, 4845-4855.

[14] Tan, C. M.; Therien, A. G.; Lu, J.; Lee, S. H.; Caron, A.; Gill, C. J.; Lebeau-Jacob, C.; Benton-Perdomo, L.; Monteiro, J. M.; Pereira, P. M.; Elsen, N. L.; Wu, J.; Deschamps, K.; Petcu, M.; Wong, S.; Daigneault, E.; Kramer, S.; Liang, L.; Maxwell, E.; Claveau, D.; Vaillancourt, J.; Skorey, K.; Tam, J.; Wang, H.; Meredith, T. C.; Sillaots, S.; Wang-Jarantow, L.; Ramtohul, Y.; Langlois, E.; Landry, F.; Reid, J. C.; Parthasarathy, G.; Sharma, S.; Baryshnikova, A.; Lumb, K. J.; Pinho, M. G.; Soisson, S. M.; Roeme, T. Restoring methicillin-resistant Staphylococcus aureus susceptibility to β-lactam antibiotics. *Science Translational Medicine* **2012**, *4*, 1-11.

[15] Kaul, M.; Zhang, Y.; Parhi, A. K.; Voie, E. J. L.; Pilch, D. S. Inhibition of RND-type efflux pumps confers the FtsZ-directed prodrug TXY436 with activity against Gram-negative bacteria. *Biochemical Pharmacology* **2014**, *89*, 321-328.

[16] Awasthi, D.; Kumar, K.; Knudson, S. E.; Slayden, R. A.; Ojima, I. SAR Studies on Trisubstituted Benzimidazoles as Inhibitors of Mtb FtsZ for the Development of Novel Antitubercular Agents. *Journal of Medicinal Chemistry* **2013,** *56*, 9756-9770.

[17] Xin, L.; Shutao, M. Advances in the discovery of novel antimicrobials targeting the assembly of bacterial cell division protein FtsZ. *European journal of medicinal chemistry* **2015**, *95*, 1-15.

[18] SunMing-Hui, J.; LiXin-Yi; WangYang; ZhangRong-Ju; YuanHan-Yu; Zhu, L.-L. Vanillin derivatives as the selective small molecule inhibitors of FtsZ**. 2014**, *23*, 2985-2994.

[19] Leung, A. K. W.; White, E. L.; Ross, L. J.; Borhani, D. W. Crystallization of the Mycobacterium tuberculosis cell-division protein FtsZ. *Acta Crystallographica Section D* **2000**, *D56,* 1634-1637.

[20] Lowe, J.; Amos, L. A. Crystal structure of the bacterial cell-division protein FtsZ. *Nature* **1998**, *391,* 203-206.

[21] Matsui, T.; Yamane, J.; Mogi, N.; Yamaguchi, H.; Takemoto, H.; Yao, M.; Tanaka, I. Structural reorganization of the bacterial cell-division protein FtsZ from Staphylococcus aureus. *Acta Crystallographica Section D* **2012**, *D68*, 1175-1188.

[22] Fujita, J.; Maeda, Y.; Mizohata, E.; Inoue, T.; Kaul, M.; Parhi, A. K.; LaVoie, E. J.; Pilch, D. S.; Matsumura, H. Structural Flexibility of an Inhibitor Overcomes Drug Resistance Mutations in Staphylococcus aureus FtsZ. *ACS Chemical Biology* **2017**, *12*, 1947-1955.

[23] Straniero, V.; Pallavicini, M.; Chiodini, G.; Ruggeri, P.; Fumagalli, L.; Bolchi, C.; Corsini, A.; Ferri, N.; Ricci, C.; Valoti, E. Farnesyltransferase inhibitors: CAAX mimetics based on different biaryl scaffolds. *Bioorganic & Medicinal Chemistry Letters* **2014**, *24*, 2924-2927.

[24] Bolchi, C.; Pallavicini, M.; Bernini, S. K.; Chiodini, G.; Corsini, A.; Ferri, N.; Fumagalli, L.; Straniero, V.; Valoti, E. Thiazole- and imidazole-containing peptidomimetic inhibitors of protein farnesyltransferase. *Bioorganic & medicinal chemistry letters* **2011**, *21*, 5408-5412.

[25] Vistoli, G.; Straniero, V.; Pedretti, A.; Fumagalli, L.; Bolchi, C.; Pallavicini, M.; Valoti, E.; Testa, B. Predicting the physicochemical profile of diastereoisomeric histidine-containing dipeptides by property space analysis. *Chirality* **2012**, *24*, 566-576.

[26] Fumagalli, L.; Pallavicini, M.; Budriesi, R.; Bolchi, C.; Canovi, M.; Chiarini, A.; Chiodini, G.; Gobbi, M.; Laurino, P.; Micucci, M.; Straniero, V.; Valoti, E. 6-Methoxy-7-benzofuranoxy and 6-Methoxy-7-indolyloxy Analogues of 2-[2-(2,6-Dimethoxyphenoxy)ethyl]aminomethyl-1,4-benzodioxane (WB4101):1 Discovery of a Potent and Selective α1D-Adrenoceptor Antagonist. *Journal of Medicinal Chemistry* **2013**, *56*, 6402-6412.

[27] Chiodini, G.; Pallavicini, M.; Zanotto, C.; Bissa, M.; Radaelli, A.; Straniero, V.; Bolchi, C.; Fumagalli, L.; Ruggeri, P.; Morghen, C. D. G. Benzodioxane–benzamides as new bacterial cell division inhibitors. *European journal of medicinal chemistry* **2015**, *89*, 252-265.

[28] Straniero, V.; Pallavicini, M.; Chiodini, G.; Zanotto, C.; Volontè, L.; Radaelli, A.; Bolchi, C.; Fumagalli, L.; Sanguinetti, M.; Menchinelli, G. 3-(Benzodioxan-2-ylmethoxy)-2, 6-difluorobenzamides bearing hydrophobic substituents at the 7-position of the benzodioxane nucleus potently inhibit methicillin-resistant Sa and Mtb cell division. *European journal of medicinal chemistry* **2016**, *120*, 227-243.

[29] Straniero, V.; Zanotto, C.; Straniero, L.; Casiraghi, A.; Duga, S.; Radaelli, A.; De Giuli Morghen, C.; Valoti, E. 2, 6-Difluorobenzamide inhibitors of the bacterial cell division protein FtsZ: design, synthesis and Structure Activity Relationship study. *ChemMedChem* **2017**, *12*, 1303-1318.

[30] Kusuma, K. D.; Payne, M.; Ung, A. T.; Bottomley, A. L.; Harry, E. J. FtsZ as an Antibacterial Target: Status and Guidelines for Progressing This Avenue. *ACS Infectious Diseases* **2019**, *5,* 1279-1294.

[31] Tripathy, S.; Sahu, S. K. FtsZ inhibitors as a new genera of antibacterial agents. *Bioorganic Chemistry*, **2019**, *91*, 103169.

[32] Xie, A.; Zhang, Q.; Liu, Y.; Feng, L.; Hu, X.; Dong, W. An Environmentally Friendly Method for N-Methylation of 5-Substituted 1H-Tetrazoles with a Green Methylating Reagent: Dimethyl Carbonate. *Journal of Heterocyclic Chemistry* **2015**, *52,* 1483-1487.

[33] Begtrup, M. Introduction of substituents into 5-membered aza-heteroaromatics. *Bulletin des Societes Chimiques Belges* **1988,** *97*, 573-598.

[34] Czaplewski, L. G.; Collins, I.; Boyd, E. A.; Brown, D.; East, S. P.; Gardiner, M.; Fletcher, R.; Haydon, D. J.; Henstock, V.; Ingram, P.; Jones, C.; Noula, C.; Kennison, L.; Rockley, C.; Rose, V.; Thomaides-Brears, H. B.; Ure, R.; Whittaker, M.; Stokes, N. R. Antibacterial alkoxybenzamide inhibitors of the essential bacterial cell division protein FtsZ, *Bioorganic & Medicinal Chemistry Letters*, **2009**, *19*, 524-527.

[35] QikProp, v. 4.1; Schrödinger, LLC: New York, **2014.**

[36] Radoux, C. J.; Olsson, T. S.; Pitt, W. R.; Groom, C. R.; Blundell, T. L. Identifying interactions that determine fragment binding at protein hotspots. *J Med Chem* **2016**, *59,* 4314-4325.

[37] Bissa, M.; Zanotto, C.; Pacchioni, S.; Volonté, L.; Venuti, A.; Lembo, D.; De Giuli Morghen, C.; Radaelli, A. The L1 protein of human papilloma virus 16 expressed by a fowlpox virus recombinant can assemble into virus-like particles in mammalian cell lines but elicits a non-neutralising humoral response, *Antivir. Res.* **2015**, *116*, 67-75.

[38] Schrödinger Release **2015**-4: LigPrep, Schrödinger, LLC, New York, NY, 2015.

[39] Jorgensen, W. L.; Maxwell, D. S.; Tirado-Rives, J. Development and testing of the OPLS all-atom force field on conformational energetics and properties of organic liquids. *J Am Chem Soc* **1996**, *118,* 11225-11236.

[40] Banks, J. L.; Beard, H. S.; Cao, Y.; Cho, A. E.; Damm, W.; Farid, R.; Felts, A. K.; Halgren, T. A.; Mainz, D. T.; Maple, J. R.; Murphy, R.; Philipp, D. M.; Repasky, M. P.; Zhang, L. Y.; Berne, B. J.; Friesner, R. A.; Gallicchio, E.; Levy, R. M. Integrated modeling program, applied chemical theory (IMPACT). *J Comput Chem* **2005,** *26*, 1752-1780.

[41] Berman, H. M.; Westbrook, J.; Feng, Z.; Gilliland, G.; Bhat, T. N.; Weissig, H.; Shindyalov, I. N.; Bourne, P. E. The Protein Data Bank. *Nucleic acids research* **2000**, *28,* 235-242.

[42] Sastry, G. M.; Adzhigirey, M.; Day, T.; Annabhimoju, R.; Sherman, W. Protein and ligand preparation: parameters, protocols, and influence on virtual screening enrichments. *Journal of computer-aided molecular design* **2013**, *27*, 221-234.

[43] Schrödinger Release **2015**-4: Maestro, Schrödinger, LLC, New York, NY, 2015.

[44] Lipinski, C. A.; Lombardo, F.; Dominy, B. W.; Feeney, P. J. Experimental and computational approaches to estimate solubility and permeability in drug discovery and development settings. *Advanced drug delivery reviews* **2001**, *46*, 3-26.

[45] Jorgensen, W. L. Efficient drug lead discovery and optimization. *Accounts of chemical research* **2009**, *42*, 724-733.

[46] Schrödinger Release **2015**-4: Glide, Schrödinger, LLC, New York, NY, 2015.

[47] Sherman, W.; Day, T.; Jacobson, M. P.; Friesner, R. A.; Farid, R., Novel procedure for modeling ligand/receptor induced fit effects. *J Med Chem* **2006**, *49* (2), 534-53.

[48] Farid, R.; Day, T.; Friesner, R. A.; Pearlstein, R. A., New insights about HERG blockade obtained from protein modeling, potential energy mapping, and docking studies. *Bioorg Med Chem* **2006**, *14* (9), 3160-3173.

[49] Friesner, R. A.; Murphy, R. B.; Repasky, M. P.; Frye, L. L.; Greenwood, J. R.; Halgren, T. A.; Sanschagrin, P. C.; Mainz, D. T., Extra precision glide: docking and scoring incorporating a model of hydrophobic enclosure for protein-ligand complexes. *J Med Chem* **2006**, *49* (21), 6177-6196.

[50] Glide, S., Schrödinger Release 2015-4; LLC, New York, NY, 2015

[51] Jacobson, M. P.; Friesner, R. A.; Xiang, Z.; Honig, B., On the role of the crystal environment in determining protein side-chain conformations. *J Mol Biol* **2002**, *320* (3), 597-608.

[52] Friesner, R. A.; Banks, J. L.; Murphy, R. B.; Halgren, T. A.; Klicic, J. J.; Mainz, D. T.; Repasky, M. P.; Knoll, E. H.; Shelley, M.; Perry, J. K.; Shaw, D. E.; Francis, P.; Shenkin, P. S., Glide: a new approach for rapid, accurate docking and scoring. 1. Method and assessment of docking accuracy. *J Med Chem* **2004**, *47* (7), 1739-1749.

WILEY-VCH

Entry for the Table of Contents

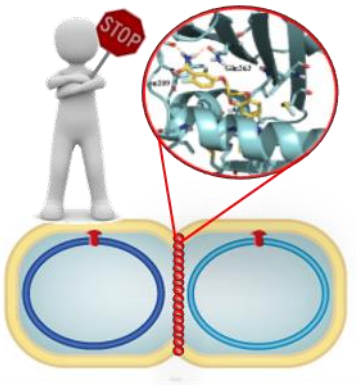

In this work, we summarize our recent findings in the SAR of a series of benzamide inhibitors of the prokaryotic cell division protein FtsZ. The proposed compounds exhibit promising activity against Gram-positive and Gram-negative strains, including multi drug resistant bacteria. We also validate a FtsZ binding protocol and highlight the key structural features for the optimal interaction with the target protein.

WILEY-VCH